Intelligent Power Control System of Three-Phase Grid-Connected PV System

Prof. Faa-Jeng Lin and Dr. Kuang-Chin Lu

linfj@ee.ncu.edu.tw

Oct. 11, 2016

Abstract

- A PC-based intelligent power control system of the three-phase grid-connected photovoltaic (PV) system for active and reactive power control during grid faults is developed.
- Considering low voltage ride through (LVRT) requirements and current limit of three-phase inverter.
- Two fuzzy-neural-network (FNN) based intelligent controllers are proposed.
  - Probabilistic wavelet fuzzy neural network (PWFNN) controller
  - Takagi-Sugeno-Kang type probabilistic fuzzy neural network with asymmetric membership function (TSKPFNN-AMF) controller
- A dual mode operation control method of the converter and inverter of the three-phase grid-connected PV system is proposed.
- Various types of voltage sags and test scenarios are designed to investigate the LVRT capability of the grid-connected PV system.
- The control performances of the proposed controllers are superior to other controllers.
  - Higher complexity of structure and current harmonic distortion of injected current during grid faults are the main defects.

Contents

Background

- The price of the photovoltaic (PV) system declines of around **75%** in less than 10 years.
- The cumulative installed capacity of the world has been reached to **178 GW** in the end of **2014.**
- EPIA predicts the worldwide total installed capacity of the PV system in **2019** could reach between 396 and 540 GW with the highest probability scenario being around **450 GW.**
- Taiwan has decided to raise the official PV installation target from **13 GW** to **20 GW** in 2025 (currently, **728 MW**).

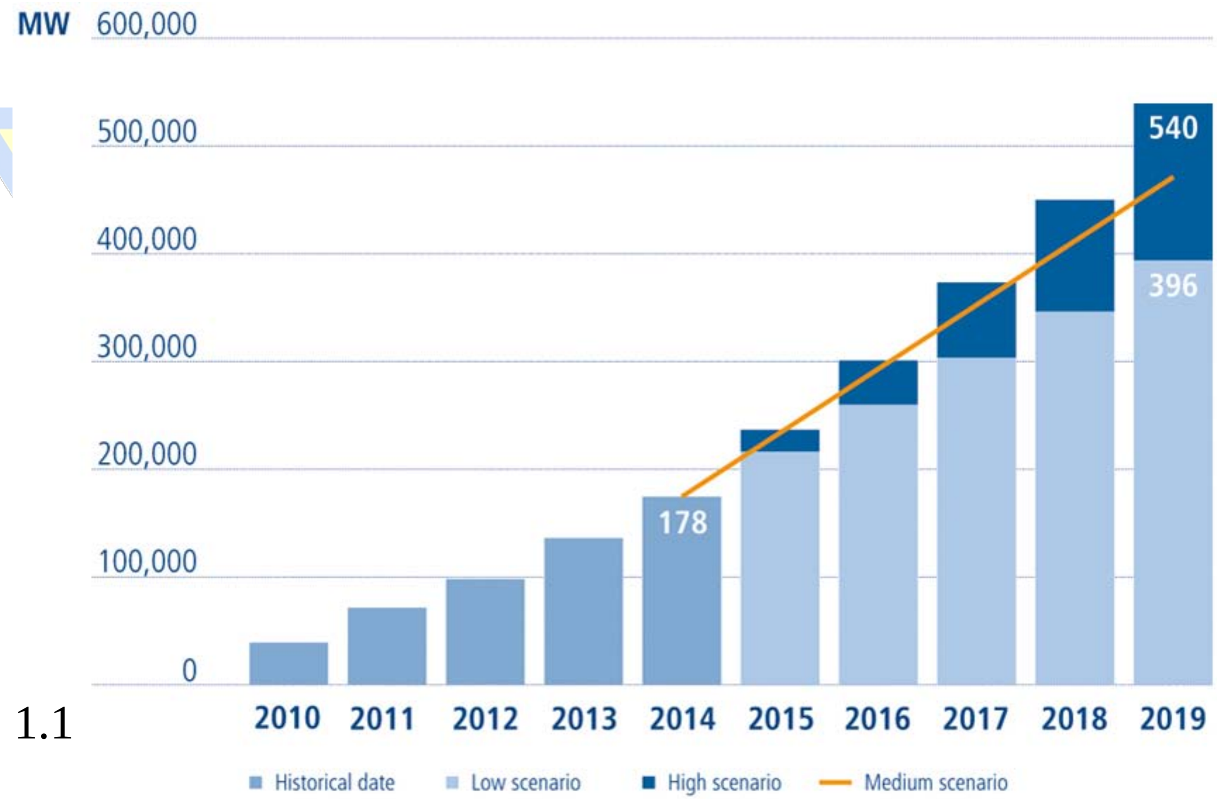

Fig. 1.1

Background

- A grid-connected PV system is mainly composed of two parts: (1) PV panel, (2) inverter.
- Optional elements:
  - Transformer (In Spain, the transformer is mandatory for galvanic isolation requirement).
  - DC-DC boost converter.
- Single-stage or two-stage
  - **Single-stage:** mainly used for medium or high power applications
    - **Pros:** simple-structure, reliable and efficient energy conversion.
    - **Cons:** higher dc-link voltage , efficiency worsened by the less accurate MPPT, partial shading issue.
  - **Two-stage:** mainly adopted in residential PV applications
    - **Pros:** place with partial shading, complicated roof structures, small space, various roof orientations.
    - **Cons:** efficiency may be lowered by the DC-DC stage, compensated by the accuracy MPPT, cost.

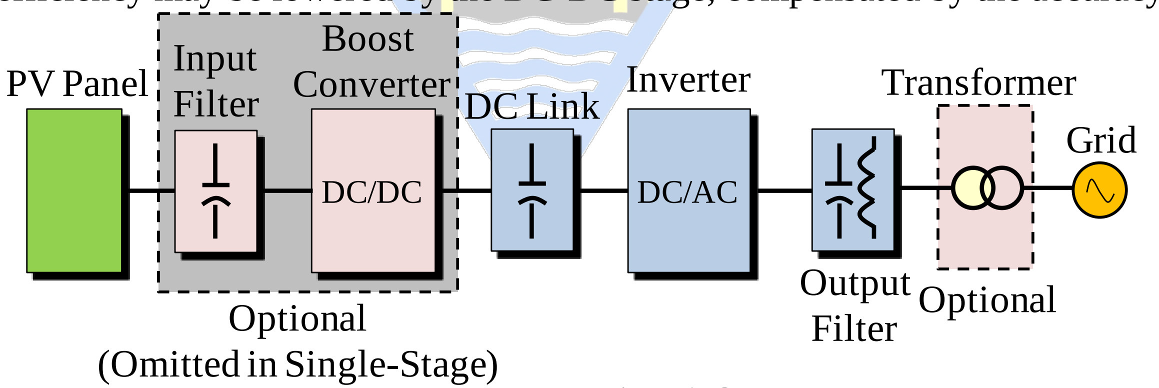

Fig. 1.2

Electrical Characteristic of PV Cell

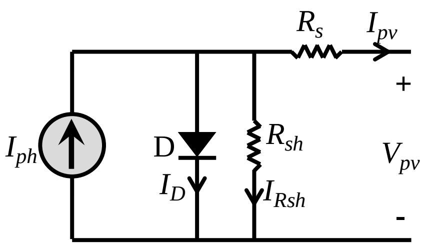

Fig. 1.3

$$P_{pv} = I_{pv}V_{pv} = I_{ph}V_{pv} - I_{rs}V_{pv}\left[\exp\left(\frac{V_{pv}}{AV_T}\right)-1\right] \quad (1.5)$$

- The short circuit current of the PV panel highly depends on the irradiance.
- High irradiance leads to large short circuit current.
- High temperature leads to small open circuit voltage.

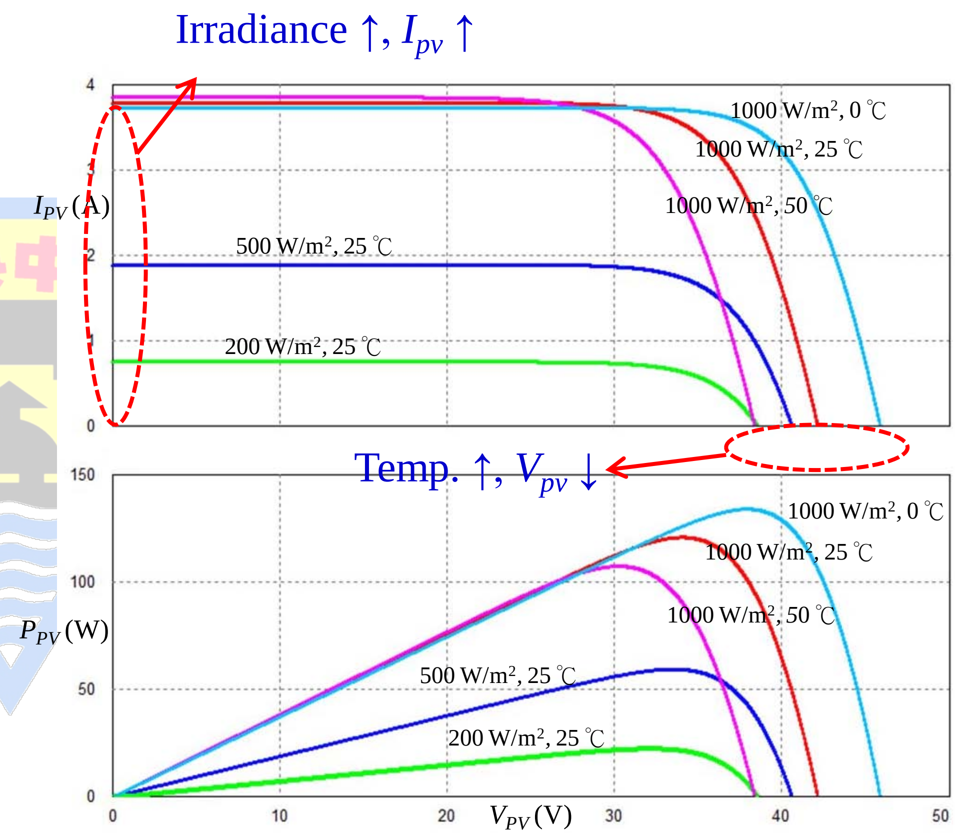

Fig. 1.4

Contents

Three-Phase Grid-Connected PV System

- PV panel is emulated by Chroma 62100H- 600S (153 VDC, 1 kW); Utility grid is emulated by KIKUSUI PCR2000LE AC power (3×2kVA)
- Y-connected 100Ω/phase resistive load, 1 kVA three-phase inverter, 3 kVA Y-△ step-up transformer.
- 16-bit A/D converter (PCI-1716), 12-bit D/A converter (MRC-6810)

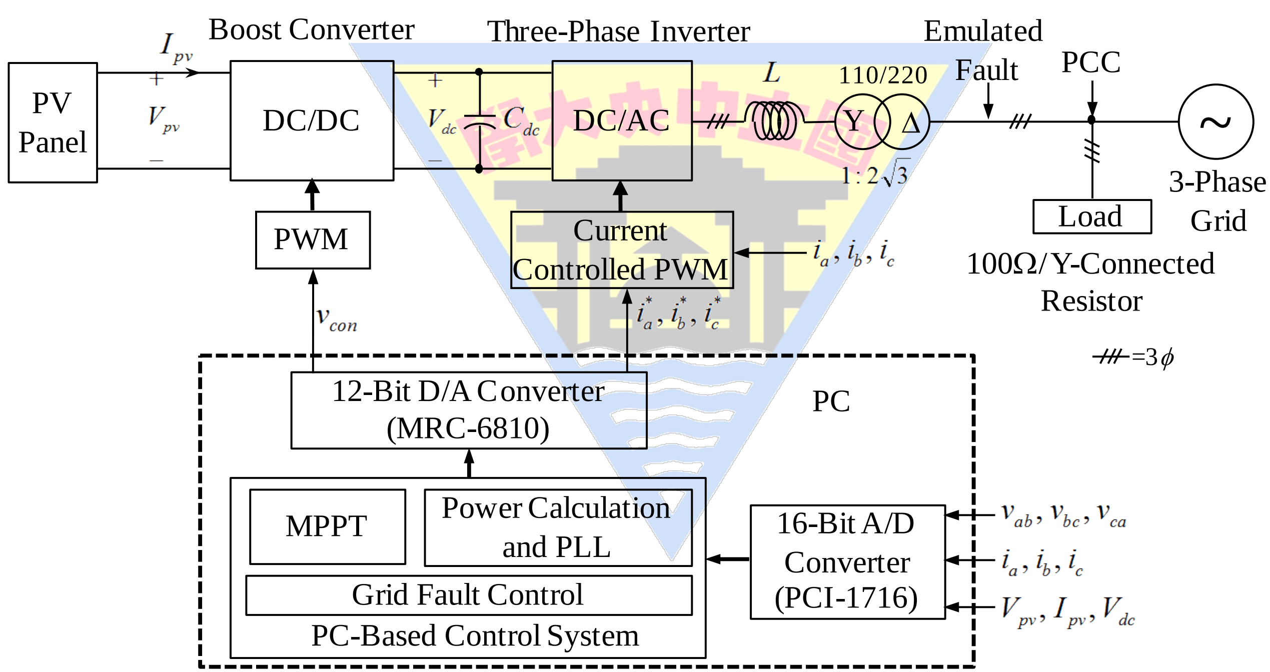

Fig. 2.1

Three-Phase Grid-Connected PV System

Table 2.1 Parameters of experimental setup.

dc-link voltage	V_{dc}	200 V
dc-link capacitor	C_{dc}	3360 μF
grid connection inductor	L	10 mH
inverter output voltage	v_{ab}, v_{bc}, v_{ca}	110 Vrms line-to-line, 60 Hz
inverter maximum current	$I_{\max}$	5 Arms (7.1 A peak current)
emulated PV panel		V_{oc}: 185.6 V, I_{sc}: 6.6 A, 1 kW
switching frequency	f_{sw_C}, f_{sw_I}	18 kHz, 10 kHz

Table 2.2 Specifications of KIKUSUI PCR2000LE.

input voltage /frequency (AC)	170~250 Vrms /47~63 Hz
output capacity	single-phase 2 kVA
voltage	output L range:1 to 150 Vrms output H range:2 to 300 Vrms
voltage resolution	0.1 Vrms
maximum output current	output L range (100 Vrms):20 A output H range (200 Vrms):10 A
maximum reverse current	30% of maximum current
frequency	1Hz~999Hz
frequency resolution	0.01Hz(1.00 Hz to 100.00 Hz) 0.1Hz(100.0 Hz to 999.9 Hz)

Three-Phase Grid-Connected PV System

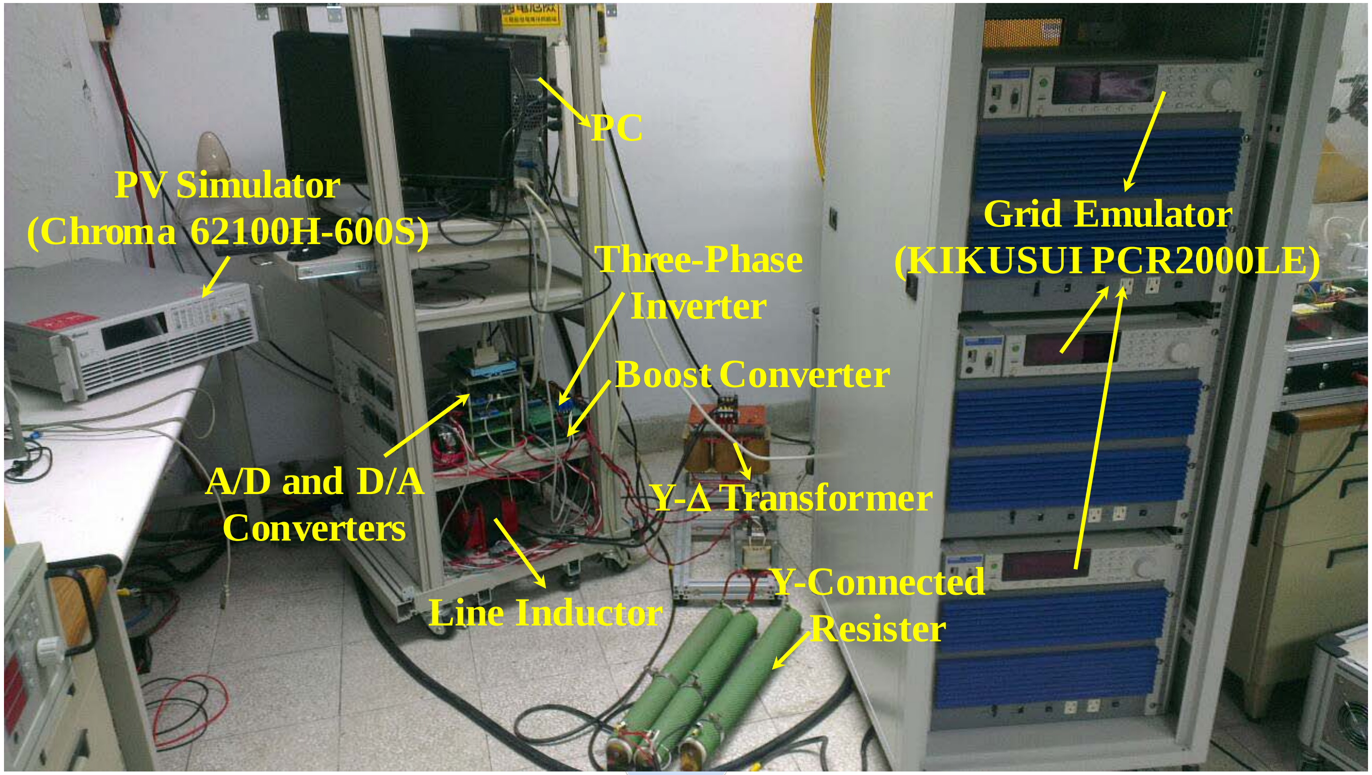

Fig. 2.5

PC-Based Control System

- MPPT control
  - voltage-based perturb-and-observe scheme (output: voltage command V_{pv}^{*}).
- Power calculation and phase-locked loop (PLL) block
  - SRF-PLL.
- Grid fault control
- Control outputs of the PC-based control system: the boost converter PWM control signal v_{con} and the three-phase inverter reference currents i_a^*, i_b^*, i_c^* .
- The SIMULINK control package is adopted for the implementation of the proposed algorithms.
- The proposed intelligent controllers are all realized using the “C” language.

Requirements of LVRT

- PV systems are largely and widely penetrated into the utility grid in recent year.
  - PV systems may stop the operation or be in unstable operation simultaneously due to transient disturbances.
  - These matters may seriously impact on the stability of the grid, such as power outage, voltage flicker.
- The next-generation PV systems have to provide a full range of services as what the traditional power plants do.
  - Low voltage ride through (LVRT) capability under grid faults.
  - Keeping connected during grid faults.
  - Support the grid by supplying reactive power during grid fault.
- E.ON requires the PV system to support voltage with additional reactive current during voltage sag.
  - The voltage control must take place within 20 ms (one cycle in Europe) after fault occurrence.
  - The amount of the additional reactive current is 2% of the rated current for each percent of the voltage sag.

Requirements of LVRT

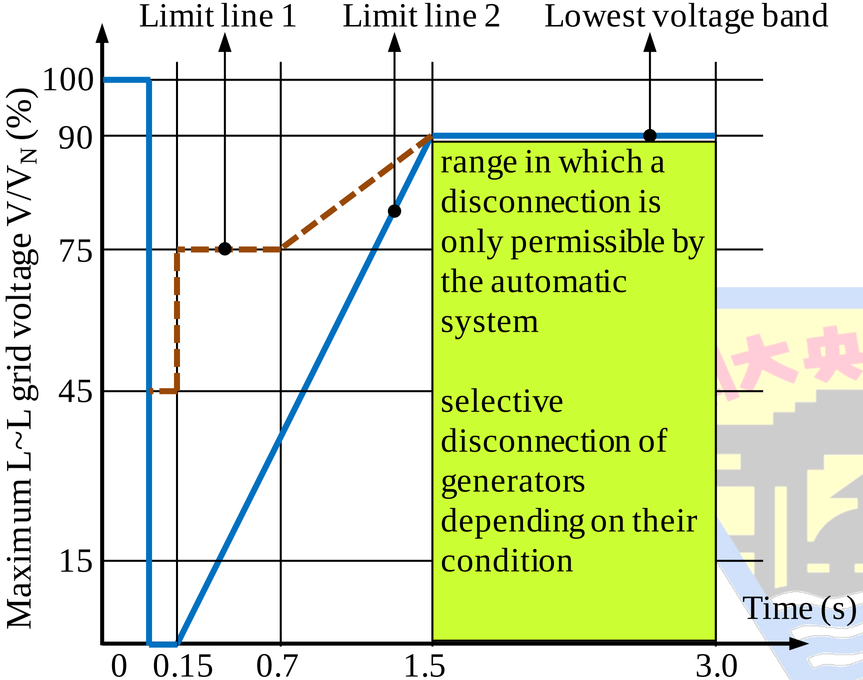

Fig. 2.6

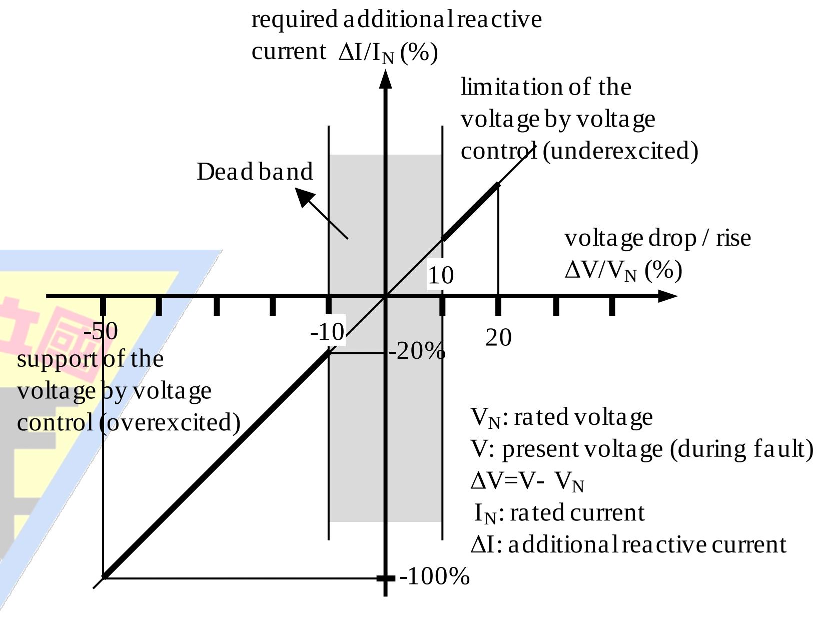

Fig. 2.7

Contents

Power Formulations

$$\begin{bmatrix} v_a \\ v_b \\ v_c \end{bmatrix} = \frac{1}{3}\begin{bmatrix} 1 & 0 & -1 \\ -1 & 1 & 0 \\ 0 & -1 & 1 \end{bmatrix}\begin{bmatrix} v_{ab} \\ v_{bc} \\ v_{ca} \end{bmatrix} \tag{3.1}$$

$$v_{\alpha\beta} = \begin{bmatrix} v_\alpha \\ v_\beta \end{bmatrix} = \frac{2}{3}\begin{bmatrix} 1 & -\frac{1}{2} & -\frac{1}{2} \\ 0 & \frac{\sqrt{3}}{2} & -\frac{\sqrt{3}}{2} \end{bmatrix}\begin{bmatrix} v_a \\ v_b \\ v_c \end{bmatrix} \tag{3.2}$$

$$\begin{bmatrix} v_d \\ v_q \end{bmatrix} = \begin{bmatrix} \cos(\theta_e) & \sin(\theta_e) \\ -\sin(\theta_e) & \cos(\theta_e) \end{bmatrix}\begin{bmatrix} v_\alpha \\ v_\beta \end{bmatrix} \tag{3.3}$$

$$\begin{bmatrix} i_d \\ i_q \end{bmatrix} = \frac{2}{3}\begin{bmatrix} \cos(\theta_e) & \cos(\theta_e - \frac{2}{3}\pi) & \cos(\theta_e + \frac{2}{3}\pi) \\ -\sin(\theta_e) & -\sin(\theta_e - \frac{2}{3}\pi) & -\sin(\theta_e + \frac{2}{3}\pi) \end{bmatrix}\begin{bmatrix} i_a \\ i_b \\ i_c \end{bmatrix} \tag{3.4}$$

$$P = \frac{3}{2}(v_d i_d + v_q i_q), \quad Q = \frac{3}{2}(v_q i_d - v_d i_q) \tag{3.5}$$

$$P = \frac{3}{2} v_q i_q \quad \text{and} \quad Q = \frac{3}{2} v_q i_d \tag{3.6}$$

Accordingly, P and Q can be regulated by controlling i_q and i_d .

Reactive and Active Power Control

$$I_r^* = \begin{cases} 0\% & , V_{sag} \le 0.1 \\ 200V_{sag}\% & , 0.1 < V_{sag} \le 0.5 \\ 100\% & , V_{sag} > 0.5 \end{cases} \tag{3.7}$$

$$V_{sag} = \left(1 - \frac{\min\left(|v_a|_{rms}, |v_b|_{rms}, |v_c|_{rms} \right)}{V_{base}} \right) \text{ pu} \tag{3.8}$$

$$|S| = \left(|v_a|_{rms} + |v_b|_{rms} + |v_c|_{rms} \right) I_{\max} \tag{3.9}$$

$$Q^* = |S| I_r^* \quad \text{and} \quad P^* = |S| \sqrt{1 - I_r^{*2}} \tag{3.10}$$

v_d

Grid Synchronization

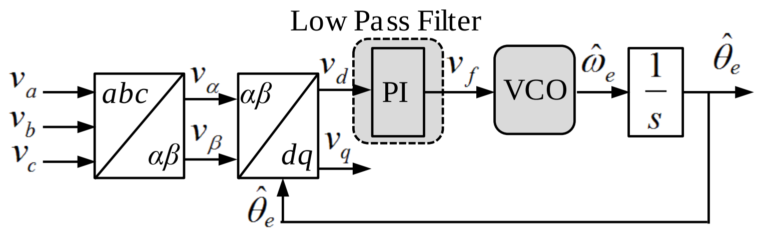

Fig. 3.1

$$\begin{bmatrix} v_a \\ v_b \\ v_c \end{bmatrix} = |V^+| \begin{bmatrix} \sin(\theta_e) \\ \sin\left(\theta_e - \frac{2}{3}\pi\right) \\ \sin\left(\theta_e + \frac{2}{3}\pi\right) \end{bmatrix} + |V^-| \begin{bmatrix} \sin(\theta_e) \\ \sin\left(\theta_e + \frac{2}{3}\pi\right) \\ \sin\left(\theta_e - \frac{2}{3}\pi\right) \end{bmatrix} \tag{3.11}$$

$$\begin{bmatrix} v_\alpha \\ v_\beta \end{bmatrix} = |V^+| \begin{bmatrix} \sin(\theta_e) \\ -\cos(\theta_e) \end{bmatrix} + |V^-| \begin{bmatrix} \sin(\theta_e) \\ \cos(\theta_e) \end{bmatrix} \tag{3.12}$$

$$\begin{bmatrix} v_d \\ v_q \end{bmatrix} = |V^+| \begin{bmatrix} \sin(\theta_e - \hat{\theta}_e) \\ -\cos(\theta_e - \hat{\theta}_e) \end{bmatrix} + |V^-| \begin{bmatrix} \sin(\theta_e + \hat{\theta}_e) \\ \cos(\theta_e + \hat{\theta}_e) \end{bmatrix} \tag{3.13}$$

The negative sequence component voltage of v_d can be filtered by using a properly designed PI low pass filter.

Dual Mode Control Strategy

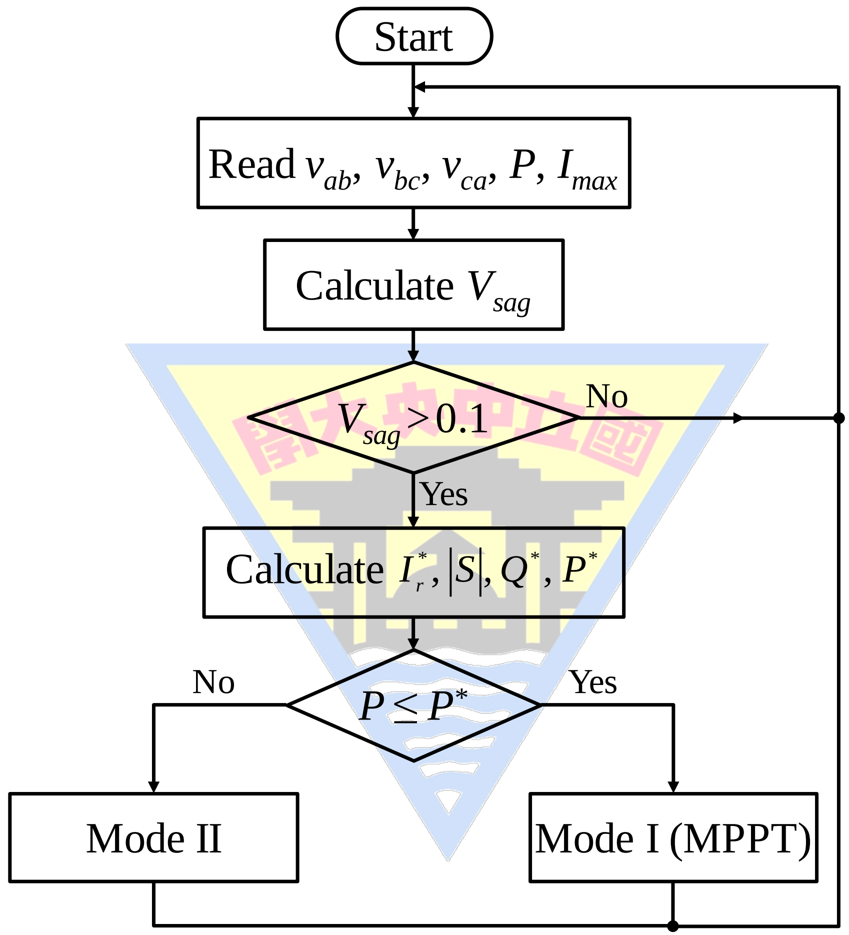

Fig. 3.2

Dual Mode Control Strategy

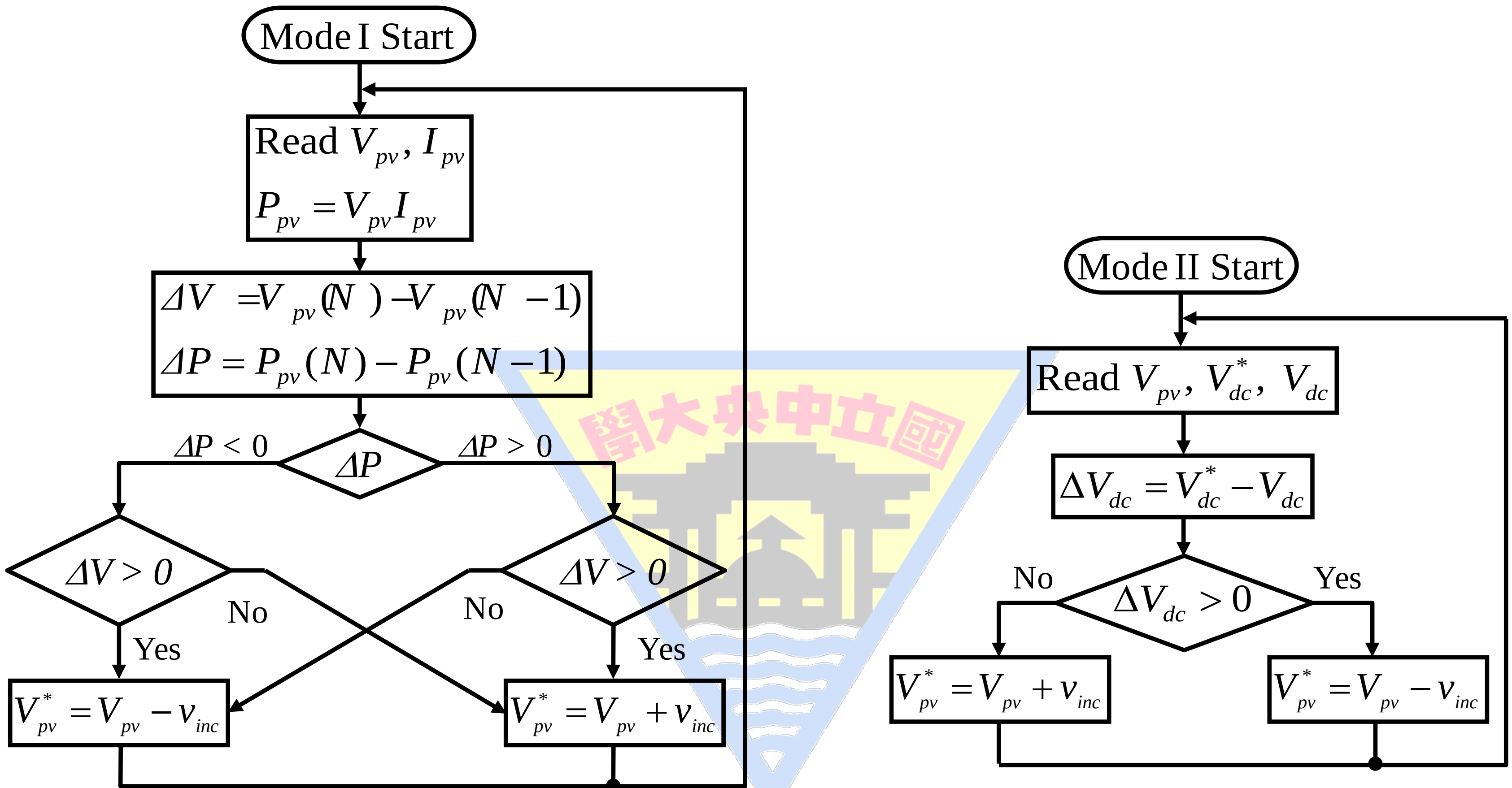

(a) (b)

Fig. 3.3

Voltage Sags Classification

- The IEEE standard 1159-1995 has defined that voltage sag is a decrease in rms voltage down to 90% to 10% of nominal voltage for a time greater than 0.5 cycles of the power frequency but less than or equal to one minute.
- “voltage sag” (in U.S.A. English) and “voltage dip” (in U.K. English) differ in meaning.

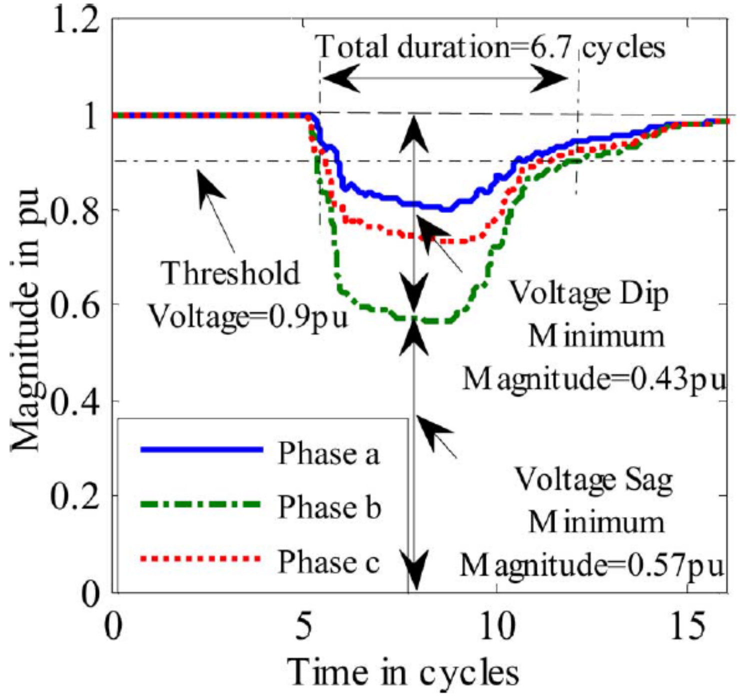

Fig. 3.4

Voltage Sags Classification

- Three-phase faults are symmetrical and called type A, which is not depicted in Fig. 3.5.
- Single phase-to-ground faults are the most common fault type.

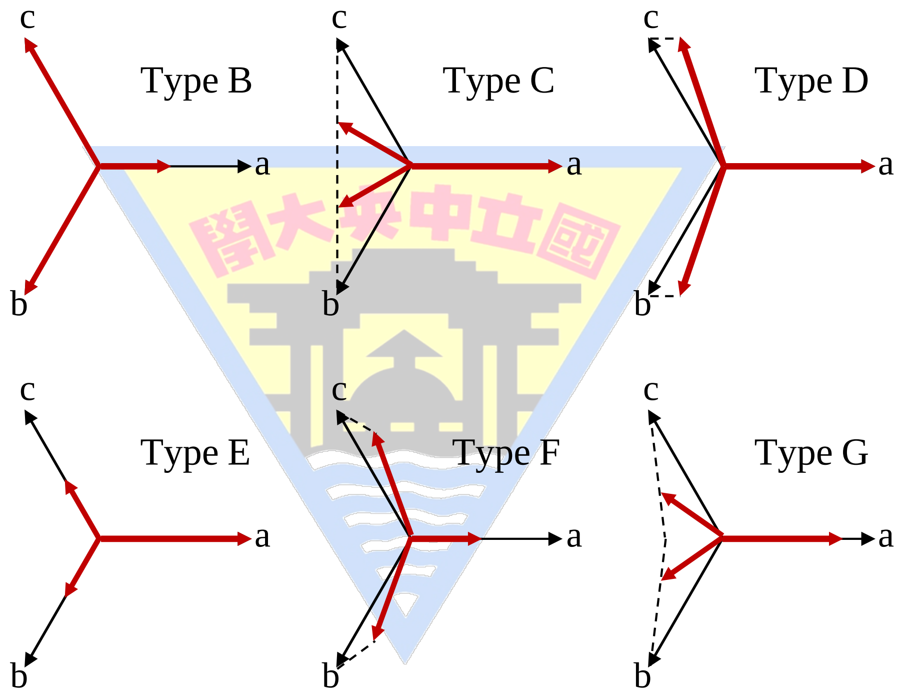

Fig. 3.5

Voltage Sags Classification

- When a fault occurs at bus 3 in Fig. 3.6, a voltage sag appears at bus 1 and propagates to bus 2 (which appears at the terminals of VSI) through the transformer (TR).
- Transformers always eliminate zero-sequence voltage and result in changing the type of voltage sag.
  - Type 1: does not change anything to voltage (e.g. Y grounded/Y grounded)
  - Type 2, which eliminates the zero-sequence voltage (e.g. Δ/Z)
  - Type 3, which swaps line and phase voltage (e.g. Δ/Y, Y/Δ, Y/Z)

Table 3.1 Transformation of voltage sags through TR

TR Type	Sag type at bus 1						
	A	B	C	D	E	F	G
	Sag type at bus 2						
Type 1	A	B	C	D	E	F	G
Type 2	A	D	C	D	G	F	G
Type 3	A	C	D	C	F	G	F

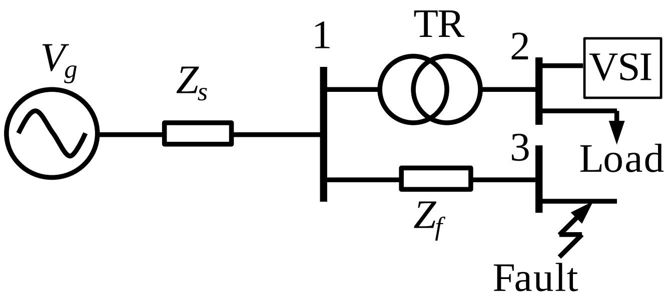

Fig. 3.6

Contents

Network Structure of PWFNN Controller

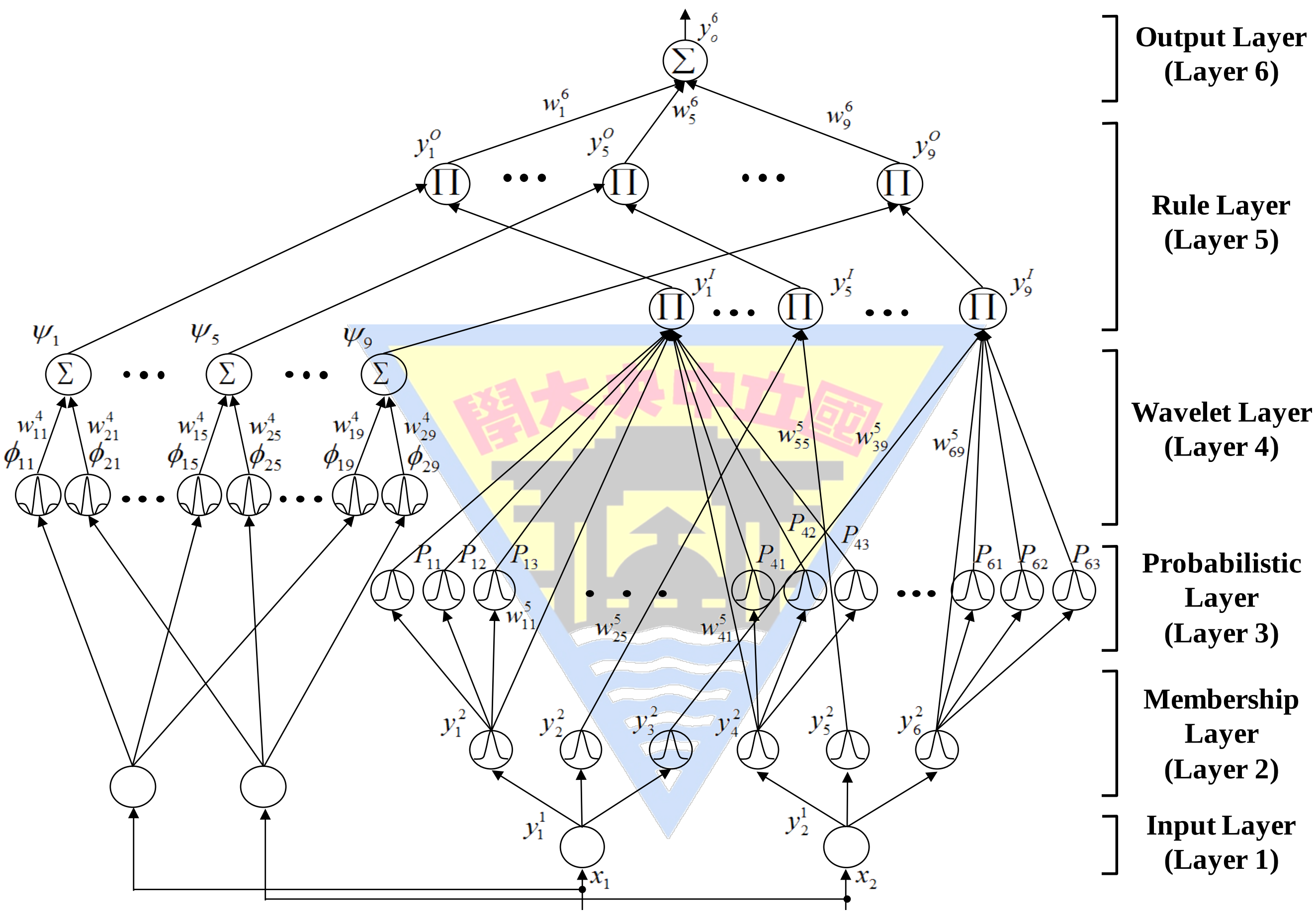

Fig. 4.1

Network Structure of PWFNN Controller

Input layer (Layer 1)

$$net_i^1(N) = x_i,\ y_i^1 = f_i^1(net_i^1(N)) = net_i^1(N), i = 1, 2 \qquad (4.1)$$

$$x_1 = e \qquad \dot{x}_1 = \dot{e} = x_2 \qquad e = V_{dc}^* - V_{dc} \text{ or } Q^* - Q$$

Membership layer (Layer 2)

$$net_j^2(N) = -\frac{(y_i^1(N) - m_j^2(N))^2}{(\sigma_j^2(N))^2}, \qquad (4.2)$$

$$y_j^2(N) = f_j^2(net_j^2(N)) = \exp\left(net_j^2(N)\right), i = 1, j = 1, 2, 3, \text{ and } i = 2, j = 4, 5, 6$$

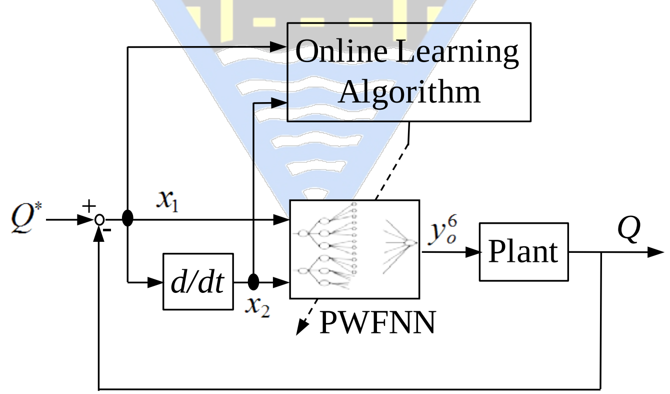

Fig. 4.2

Network Structure of PWFNN Controller

Probabilistic layer (Layer 3)

$$P_{jp}(N) = f_{jp}\left(y_j^2(N)\right) = \exp\left(-\frac{\left(y_j^2(N) - m_{jp}^3\right)^2}{\left(\sigma_{jp}^3\right)^2}\right),\ j = 1, 2, \ldots, 6,\ p = 1, 2, 3 \qquad (4.3)$$

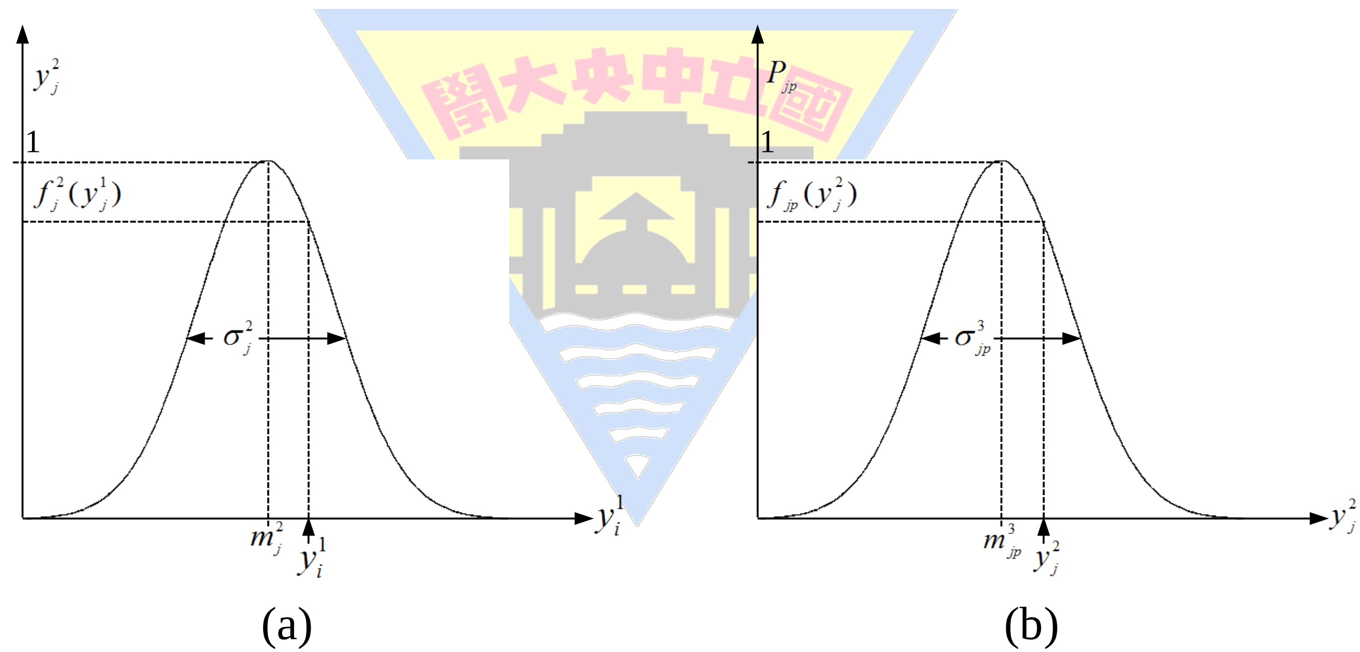

Fig. 4.3

Network Structure of PWFNN Controller

Wavelet layer (Layer 4)

$$g_{ik}(N)=\frac{\left(x_i(N)-m_{ik}^4\right)^2}{\left(\sigma_{ik}^4\right)^2},\ i=1,2,\ k=1,2,\ldots,9$$

$$\phi_{ik}(N)=\frac{1}{\sqrt{\left|\sigma_{ik}^4\right|}}\left(1-g_{ik}(N)\right)\exp\left(-\frac{g_{ik}(N)}{2}\right) \tag{4.4}$$

$$\psi_k(N)=\sum_i w_{ik}^4\phi_{ik}(N),\ i=1,2,\ k=1,2,\cdots,9 \tag{4.5}$$

Rule layer (Layer 5)

$$y_k^I(N)=\prod_{j,p} w_{jk}^5 y_j^2 P_{jp},\ k=1,2,\cdots,9,\ p=1,2,3 \tag{4.6}$$

$$y_k^O(N)=\psi_k(N)y_k^I(N),\ k=1,2,\cdots,9 \tag{4.7}$$

Output layer (Layer 6)

$$y_o^6(N)=\sum_k w_k^6(N)y_k^O(N),\ o=1;\ k=1,2,\cdots,9 \tag{4.8}$$

Online Learning Algorithm of PWFNN Controller

- Four adjustable parameters $w_k^6,\ w_{ik}^4,\ m_j^2,\ \sigma_j^2$ need to be tuned.
- The purpose of the BP algorithm is to minimize the energy function *E*

$$E(N)=\frac{1}{2}(y^*(N)-y(N))^2=\frac{1}{2}e^2(N) \qquad (4.9)$$

The gradient error of *E*

$$\delta_o^6=-\frac{\partial E}{\partial y_o^6(N)}=-\frac{\partial E}{\partial y}\frac{\partial y}{\partial y_o^6(N)} \qquad (4.10)$$

$$\Delta w_k^6=-\eta_1\frac{\partial E}{\partial w_k^6(N)}=-\eta_1\frac{\partial E}{\partial y_o^6(N)}\frac{\partial y_o^6(N)}{\partial w_k^6(N)}=\eta_1\delta_o^6 y_k^O \qquad (4.11)$$

$$w_k^6(N+1)=w_k^6(N)+\Delta w_k^6 \qquad (4.12)$$

Online Learning Algorithm of PWFNN Controller

In layer 4

$$\delta_k^4 = -\frac{\partial E}{\partial \psi_k(N)} = -\frac{\partial E}{\partial y_o^6(N)} \frac{\partial y_o^6(N)}{\partial y_k^O(N)} \frac{\partial y_k^O(N)}{\partial \psi_k(N)} = \delta_k^O y_k^I \tag{4.15}$$

$$\Delta w_{ik}^4 = -\eta_2 \frac{\partial E}{\partial w_{ik}^4(N)} = -\eta_2 \frac{\partial E}{\partial \psi_k(N)} \frac{\partial \psi_k(N)}{\partial w_{ik}^4(N)} = \eta_2 \delta_k^4 \phi_{ik} \tag{4.16}$$

$$w_{ik}^4(N+1) = w_{ik}^4(N) + \Delta w_{ik}^4 \tag{4.17}$$

In layer 2

$$\delta_j^2 = -\frac{\partial E}{\partial net_j^2(N)} = -\frac{\partial E}{\partial y_k^I(\mathrm{N})} \frac{\partial y_k^I(N)}{\partial y_j^2(N)} \frac{\partial y_j^2(N)}{\partial net_j^2(N)} = \sum_k w_{jk}^5 \delta_k^I y_k^I \tag{4.18}$$

$$\Delta m_j^2 = -\eta_3 \frac{\partial E}{\partial m_j^2} = -\eta_3 \frac{\partial E}{\partial net_j^2(N)} \frac{\partial net_j^2(N)}{\partial m_j^2(N)} = \eta_3 \delta_j^2 \frac{2(y_i^1 - m_j^2)}{(\sigma_j^2)^2} \tag{4.19}$$

$$\Delta \sigma_j^2 = -\eta_4 \frac{\partial E}{\partial \sigma_j^2} = -\eta_4 \frac{\partial E}{\partial net_j^2(N)} \frac{\partial net_j^2(N)}{\partial \sigma_j^2(N)} = \eta_4 \delta_j^2 \frac{2(y_i^1 - m_j^2)^2}{(\sigma_j^2)^2} \tag{4.20}$$

Online Learning Algorithm of PWFNN Controller

$$m_j^2(N+1) = m_j^2(N) + \Delta m_j^2 \qquad (4.21)$$

$$\sigma_j^2(N+1) = \sigma_j^2(N) + \Delta \sigma_j^2 \qquad (4.22)$$

Owing to the uncertainties of the grid-connected three-phase PV system, the exact calculation of the sensitivity of the system $\partial y / \partial y_o^6(N)$ cannot be determined exactly.

$$\delta_o^6 \cong (y^* - y) + (\dot{y}^* - \dot{y}) = e + \dot{e} \qquad (4.23)$$

Online Learning Algorithm of PWFNN Controller

Online learning algorithm of PWFNN control scheme

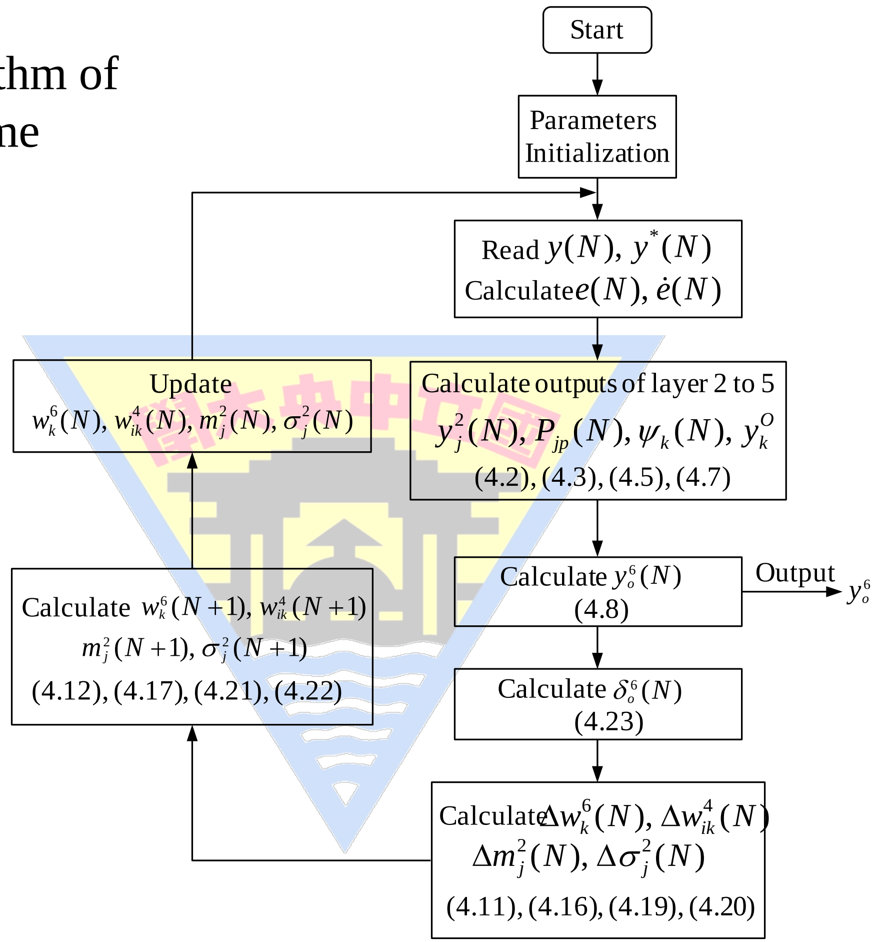

Fig. 4.4

Convergence of PWFNN controller

The resulted varied learning rates are shown in the following equations:

$$\eta_1 = \frac{E(N)/4}{R_1+\varepsilon}, \text{ where } R_1 = \sum_{k-1}^{9}\left(\frac{\partial E}{\partial y_o^6(N)}\frac{\partial y_o^6(N)}{\partial w_k^6}\right)^2 \tag{4.24}$$

$$\eta_2 = \frac{E(N)/4}{R_2+\varepsilon}, \text{ where } R_2 = \sum_{k=1}^{9}\sum_{i=1}^{2}\left[\frac{\partial E}{\partial y_o^6(N)}\frac{\partial y_o^6(N)}{\partial w_{ik}^4(N)}\right]^2 \tag{4.25}$$

$$\eta_3 = \frac{E(N)/4}{R_3+\varepsilon}, \text{ where } R_3 = \sum_{j=1}^{6}\left[\frac{\partial E}{\partial y_o^6(N)}\frac{\partial y_o^6(N)}{\partial m_j^2(N)}\right]^2 \tag{4.26}$$

$$\eta_4 = \frac{E(N)/4}{R_4+\varepsilon}, \text{ where } R_4 = \sum_{j=1}^{6}\left[\frac{\partial E}{\partial y_o^6(N)}\frac{\partial y_o^6(N)}{\partial \sigma_j^2(N)}\right]^2 \tag{4.27}$$

Convergence of PWFNN controller

$$\Delta E(N) = E(N+1) - E(N) \tag{4.28}$$

$$\begin{aligned} E(N+1) &= E(N) + \Delta E(N) \\ &\approx E(N) + \sum_{k=1}^{9}\left(\frac{\partial E(N)}{\partial w_k^6}\Delta w_k^6\right) \\ &\quad + \sum_{k=1}^{9}\sum_{i=1}^{2}\left(\frac{\partial E(N)}{\partial w_{ik}^4}\Delta w_{ik}^4\right) + \sum_{j=1}^{6}\left(\frac{\partial E(N)}{\partial m_j^2}\Delta m_j^2 + \frac{\partial E(N)}{\partial \sigma_j^2}\Delta \sigma_j^2\right) \\ &= \frac{E(N)}{4} - \eta_1 \sum_{k=1}^{9}\left(\frac{\partial E}{\partial y_o^6(N)}\frac{\partial y_o^6(N)}{\partial w_k^6}\right)^2 + \frac{E(N)}{4} - \eta_2 \sum_{k=1}^{9}\sum_{i=1}^{2}\left(\frac{\partial E}{\partial y_o^6(N)}\frac{\partial y_o^6(N)}{\partial w_{ik}^4(N)}\right)^2 \\ &\quad + \frac{E(N)}{4} - \eta_3 \sum_{j=1}^{6}\left(\frac{\partial E}{\partial y_o^6(N)}\frac{\partial y_o^6(N)}{\partial m_j^2(N)}\right)^2 + \frac{E(N)}{4} - \eta_4 \sum_{j=1}^{6}\left(\frac{\partial E}{\partial y_o^6(N)}\frac{\partial y_o^6(N)}{\partial \sigma_j^2(N)}\right)^2 \end{aligned} \tag{4.29}$$

$$\begin{aligned} E(N+1) &\approx \varepsilon\left(\sum_{m=1}^{4}\eta_m\right) = \frac{E(N)\varepsilon/4}{R_1+\varepsilon} + \frac{E(N)\varepsilon/4}{R_2+\varepsilon} \\ &\quad + \frac{E(N)\varepsilon/4}{R_3+\varepsilon} + \frac{E(N)\varepsilon/4}{R_4+\varepsilon} < E(N) \end{aligned} \tag{4.30}$$

Network Structure of TSKPFNN-AMF Controller

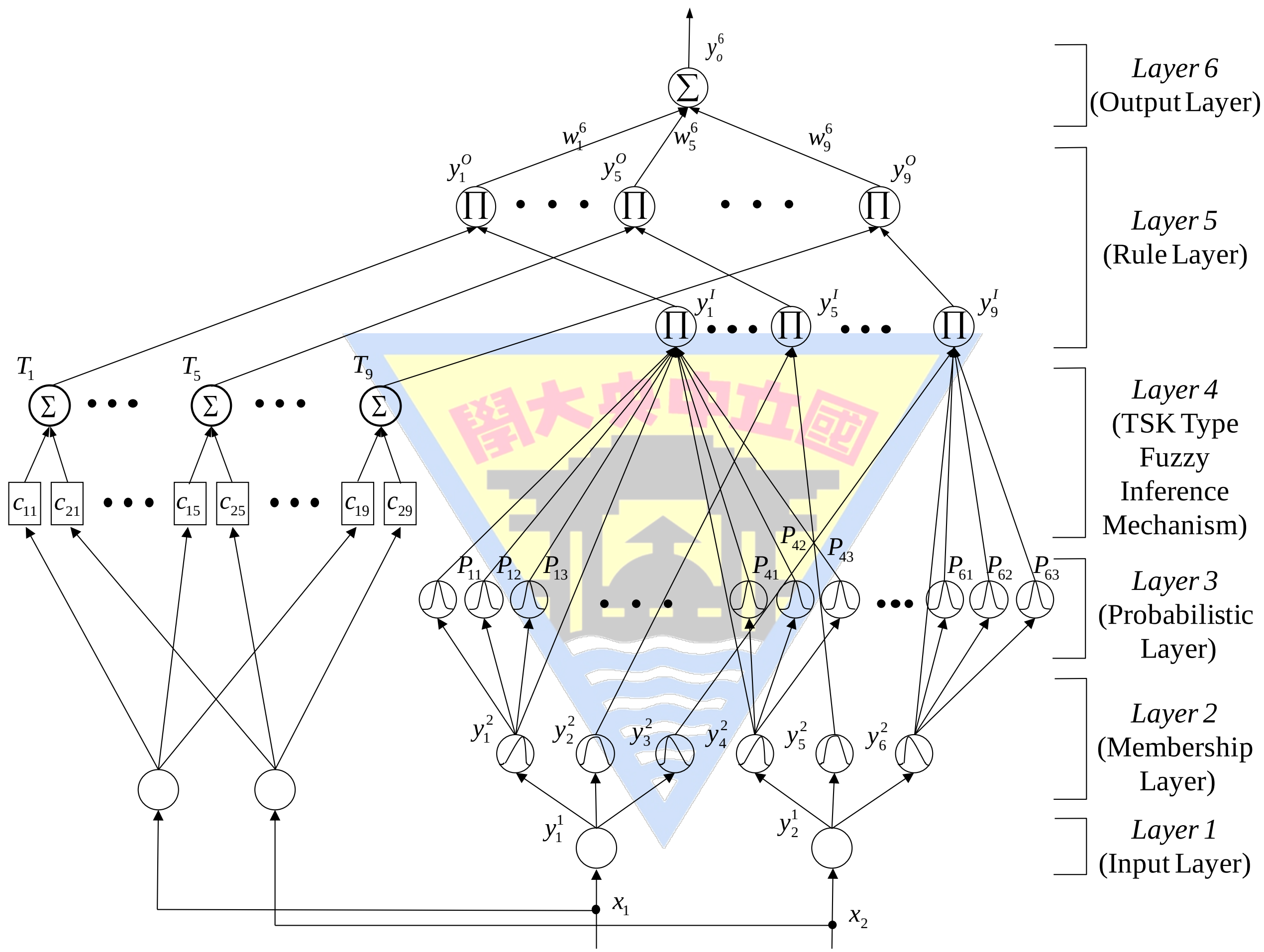

Fig. 4.5

Network Structure of TSKFNN-AMF Controller

Layer 1 (Input layer)

$$net_i^1(N) = x_i^1,\ y_i^1(N) = f_i^1(net_i^1(N)) = net_i^1(N),\ i = 1, 2 \qquad (4.32)$$

$$e = V_{dc}^* - V_{dc} \ \text{ or } P^*\text{-}P \ \text{ or } \ Q^* - Q$$

Layer 2 (Membership layer)

$$net_j^2(N) = \begin{cases} -\dfrac{(y_i^1(N) - m_j^2(N))^2}{(\sigma_{L\_j}^2(N))^2}, & -\infty < y_i^1(N) \le m_j^2 \\ -\dfrac{(y_i^1(N) - m_j^2(N))^2}{(\sigma_{R\_j}^2(N))^2}, & m_j^2 < y_i^1(N) < \infty \end{cases} \qquad (4.33)$$

$$y_j^2(N) = f_j^2(net_j^2(N)) = \exp\left(net_j^2(N)\right) \qquad (4.34)$$

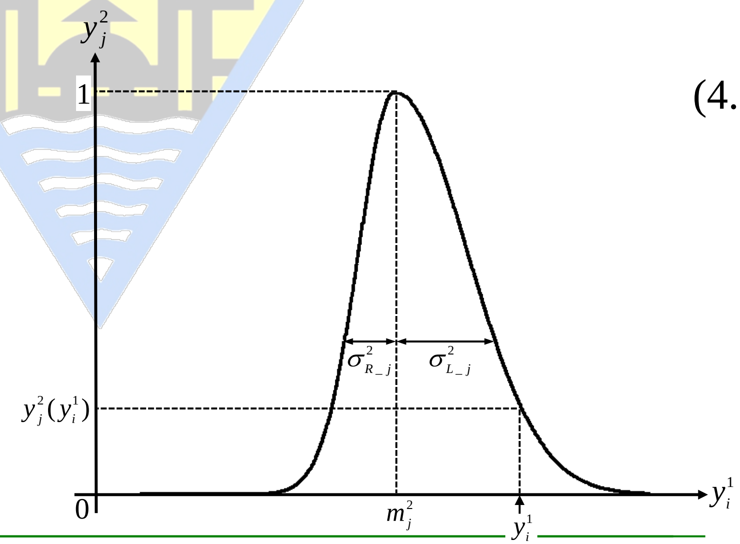

Fig. 4.6

Network Structure of TSKFNN-AMF Controller

Layer 3 (Probability layer)

$$P_{jp}(N) = f_{jp}(y_j^2(N)) = \exp\left[-\frac{(y_j^2(N) - m_{jp}^3)^2}{(\sigma_{jp}^3)^2}\right] \tag{4.35}$$

$$, \ j = 1, 2, \cdots, 6; \ p = 1, 2, 3$$

Layer 4 (TSK type fuzzy inference mechanism layer)

$$T_k(N) = \sum_i c_{ik}(N) x_i(N), \ i = 1,2; \ k = 1, 2, \cdots, 9 \tag{4.36}$$

Layer 5 (Rule layer)

$$y_k^I(N) = y_r^2(N) y_l^2(N) S_r(N) S_l(N), \ r = 1, 2, 3$$
$$; l = 4, 5, 6; \ k = 3(r-1) + (l-3) \tag{4.37}$$

$$S_j(N) = \prod_p P_{jp}(N), \ j = 1, 2, \cdots, 6; \ p = 1, 2, 3 \tag{4.38}$$

$$y_k^O(N) = T_k(N) y_k^I(N), \ k = 1, 2, \cdots, 9 \tag{4.39}$$

Layer 6 (Output layer)

$$y_o^6(N) = \sum_k w_k^6(N) y_k^O(N), \ o = 1; \ k = 1, 2, \cdots, 9 \tag{4.40}$$

Online Learning Algorithm of TSKPFNN-AMF Controller

- The purpose of the BP algorithm is to minimize the energy function E

$$E(N)=\frac{1}{2}(y^*(N)-y(N))^2=\frac{1}{2}e^2(N) \tag{4.41}$$

<u>*Layer 6*</u>

$$\delta_o^6=-\frac{\partial E}{\partial y_o^6(N)}=-\frac{\partial E}{\partial y}\frac{\partial y}{\partial y_o^6(N)} \tag{4.42}$$

$$\Delta w_k^6=-\eta_1\frac{\partial E}{\partial w_k^6(N)}=-\eta_1\frac{\partial E}{\partial y_o^6(N)}\frac{\partial y_o^6(N)}{\partial w_k^6(N)}=\eta_1\delta_o^6 y_k^O \tag{4.43}$$

$$w_k^6(N+1)=w_k^6(N)+\Delta w_k^6 \tag{4.44}$$

<u>*Layer 5*</u>

$$\delta_k^O=-\frac{\partial E}{\partial y_k^O(N)}=-\frac{\partial E}{\partial y_o^6(N)}\frac{\partial y_o^6(N)}{\partial y_k^O(N)}=\delta_o^6 w_k^6 \tag{4.45}$$

$$\delta_k^I=-\frac{\partial E}{\partial y_k^I(N)}=-\frac{\partial E}{\partial y_k^O(N)}\frac{\partial y_k^O(N)}{\partial y_k^I(N)}=\delta_k^O T_k \tag{4.46}$$

Online Learning Algorithm of TSKPFNN-AMF Controller

Layer 4

$$\delta_k^4 = -\frac{\partial E}{\partial T_k(N)} = -\frac{\partial E}{\partial y_k^O(N)} \frac{\partial y_k^O(N)}{\partial T_k(N)} = \delta_k^O y_k^I \tag{4.47}$$

$$\Delta c_{ik} = -\eta_2 \frac{\partial E}{\partial c_{ik}(N)} = -\eta_2 \frac{\partial E}{\partial T_k(N)} \frac{\partial T_k(N)}{\partial c_{ik}(N)} = \eta_2 \delta_k^4 x_i \tag{4.48}$$

$$c_{ik}(N+1) = c_{ik}(N) + \Delta c_{ik} \tag{4.49}$$

Layer 2

$$\begin{aligned}\delta_j^2 &= -\frac{\partial E}{\partial net_j^2(N)} = -\frac{\partial E}{\partial y_k^I(N)} \frac{\partial y_k^I(N)}{\partial y_j^2(N)} \frac{\partial y_j^2(N)}{\partial net_j^2(N)} \\ &= \begin{cases} h_j \sum_r \delta_k^I y_k^I, \ j = 1, 2, 3;\ r = 1, 2, 3;\ k = 3(j-1) + r \\ h_j \sum_r \delta_k^I y_k^I, \ j = 4, 5, 6;\ r = 1, 2, 3;\ k = j + 3(r-2) \end{cases}\end{aligned} \tag{4.50}$$

$$h_j = 1 - y_j^2 \sum_p \frac{y_j^2 - m_{jp}^3}{(\sigma_{jp}^3)^2}, \ p = 1, 2, 3 \tag{4.51}$$

Online Learning Algorithm of TSKPFNN-AMF Controller

$$\Delta m_j^2 = -\eta_3 \frac{\partial E}{\partial m_j^2} = -\eta_3 \frac{\partial E}{\partial net_j^2(N)} \frac{\partial net_j^2(N)}{\partial m_j^2(N)}$$

$$= \begin{cases} \eta_3 \delta_j^2 \dfrac{2(y_i^1 - m_j^2)}{(\sigma_{L\_j}^2)^2}, & -\infty < y_i^1 \le m_j^2,\ j = 1, 2, \cdots, 6 \\ \eta_3 \delta_j^2 \dfrac{2(y_i^1 - m_j^2)}{(\sigma_{R\_j}^2)^2}, & m_j^2 < y_i^1 < \infty,\ j = 1, 2, \cdots, 6 \end{cases} \tag{4.52}$$

$$\Delta \sigma_{L\_j}^2 = -\eta_4 \frac{\partial E}{\partial \sigma_{L\_j}^2} = -\eta_4 \frac{\partial E}{\partial net_j^2(N)} \frac{\partial net_j^2(N)}{\partial \sigma_{L\_j}^2(N)}$$

$$= \eta_4 \delta_j^2 \frac{2(y_i^1 - m_j^2)^2}{(\sigma_{L\_j}^2)^3},\ j = 1, 2, \cdots, 6 \tag{4.53}$$

$$\Delta \sigma_{R\_j}^2 = -\eta_5 \frac{\partial E}{\partial \sigma_{R\_j}^2} = -\eta_5 \frac{\partial E}{\partial net_j^2(N)} \frac{\partial net_j^2(N)}{\partial \sigma_{R\_j}^2(N)}$$

$$= \eta_5 \delta_j^2 \frac{2(y_i^1 - m_j^2)^2}{(\sigma_{R\_j}^2)^3},\ j = 1, 2, \cdots, 6 \tag{4.54}$$

Online Learning Algorithm of TSKPFNN-AMF Controller

$$m_j^2(N+1) = m_j^2(N) + \Delta m_j^2 \quad (4.55)$$

$$\sigma_{L\_j}^2(N+1) = \sigma_{L\_j}^2(N) + \Delta\sigma_{L\_j}^2 \quad (4.56)$$

$$\sigma_{R\_j}^2(N+1) = \sigma_{R\_j}^2(N) + \Delta\sigma_{R\_j}^2 \quad (4.57)$$

$$\delta_o^6 \cong (y^* - y) + (\dot{y}^* - \dot{y}) = e + \dot{e} \quad (4.58)$$

Convergence Analyses of the TSKPFNN-AMF Controller

The varied learning rates based on the analysis of a discrete-type Lyapunov function have been derived as follows:

$$\eta_1 = \frac{E(N)/5}{R_1 + \varepsilon}, \text{ where } R_1 = \sum_{k=1}^{9} \left(\frac{\partial E}{\partial y_o^6(N)} \frac{\partial y_o^6(N)}{\partial w_k^6} \right)^2 \tag{4.59}$$

$$\eta_2 = \frac{E(N)/5}{R_2 + \varepsilon}, \text{ where } R_2 = \sum_{k=1}^{9} \sum_{i=1}^{2} \left(\frac{\partial E}{\partial T_k(N)} \frac{\partial T_k(N)}{\partial c_{ik}} \right)^2 \tag{4.60}$$

$$\eta_3 = \frac{E(N)/5}{R_3 + \varepsilon}, \text{ where } R_3 = \sum_{j=1}^{6} \left(\frac{\partial E}{\partial net_j^2(N)} \frac{\partial net_j^2(N)}{\partial m_j^2(N)} \right)^2 \tag{4.61}$$

$$\eta_4 = \frac{E(N)/5}{R_4 + \varepsilon}, \text{ where } R_4 = \sum_{j=1}^{6} \left(\frac{\partial E}{\partial net_j^2(N)} \frac{\partial net_j^2(N)}{\partial \sigma_{L\_j}^2(N)} \right)^2 \tag{4.62}$$

$$\eta_5 = \frac{E(N)/5}{R_5 + \varepsilon}, \text{ where } R_5 = \sum_{j=1}^{6} \left(\frac{\partial E}{\partial net_j^2(N)} \frac{\partial net_j^2(N)}{\partial \sigma_{R\_j}^2(N)} \right)^2 \tag{4.63}$$

Convergence Analyses of the TSKPFNN-AMF Controller

The change in the Lyapunov function can be written as

$$\Delta E(N) = E(N+1) - E(N) \tag{4.64}$$

$$\begin{aligned}
E(N+1) &= E(N) + \Delta E(N) \\
&\approx E(N) + \sum_{k=1}^{9}\left(\frac{\partial E(N)}{\partial w_k^6}\Delta w_k^6\right) + \sum_{k=1}^{9}\sum_{i=1}^{2}\left(\frac{\partial E(N)}{\partial c_{ik}}\Delta c_{ik}\right) \\
&\quad + \sum_{j=1}^{6}\left(\frac{\partial E(N)}{\partial m_j^2}\Delta m_j^2\right) + \sum_{j=1}^{6}\left(\frac{\partial E(N)}{\partial \sigma_{L_j}^2}\Delta \sigma_{L_j}^2 + \frac{\partial E(N)}{\partial \sigma_{R_j}^2}\Delta \sigma_{R_j}^2\right) \\
&= \frac{E(N)}{5} - \eta_1 \sum_{k=1}^{9}\left(\frac{\partial E}{\partial y_o^6(N)}\frac{\partial y_o^6(N)}{\partial w_k^6}\right)^2 + \frac{E(N)}{5} - \eta_2 \sum_{k=1}^{9}\sum_{i=1}^{2}\left(\frac{\partial E}{\partial T_k(N)}\frac{\partial T_k(N)}{\partial c_{ik}(N)}\right)^2 \\
&\quad + \frac{E(N)}{5} - \eta_3 \sum_{j=1}^{6}\left(\frac{\partial E}{\partial net_j^2(N)}\frac{\partial net_j^2(N)}{\partial m_j^2(N)}\right)^2 + \frac{E(N)}{5} - \eta_4 \sum_{j=1}^{6}\left(\frac{\partial E}{\partial net_j^2(N)}\frac{\partial net_j^2(N)}{\partial \sigma_{L_j}^2(N)}\right)^2 \\
&\quad + \frac{E(N)}{5} - \eta_5 \sum_{j=1}^{6}\left(\frac{\partial E}{\partial net_j^2(N)}\frac{\partial net_j^2(N)}{\partial \sigma_{R_j}^2(N)}\right)
\end{aligned} \tag{4.65}$$

Convergence Analyses of the TSKPFNN-AMF Controller

If the learning rates of the TSKPFNN-AMF controller are designed as (4.59) to (4.63), then (4.65) can be rewritten as

$$E(N+1) \approx \varepsilon(\sum_{m=1}^{5}\eta_m) = \frac{E(N)\varepsilon/5}{R_1+\varepsilon} + \frac{E(N)\varepsilon/5}{R_2+\varepsilon} + \frac{E(N)\varepsilon/5}{R_3+\varepsilon} + \frac{E(N)\varepsilon/5}{R_4+\varepsilon} + \frac{E(N)\varepsilon/5}{R_5+\varepsilon} < E(N) \tag{4.66}$$

$$\Delta E(N) \approx \varepsilon\left(\sum_{m=1}^{5}\eta_m\right) - E(N) = \frac{E(N)}{5}\left[\sum_{m=1}^{5}\left(\frac{\varepsilon}{R_m+\varepsilon}-1\right)\right] = -\frac{E(N)}{5}\left[\sum_{m=1}^{5}\left(\frac{R_m}{R_m+\varepsilon}\right)\right] < 0 \tag{4.67}$$

Therefore, the proof of the convergence of TSKPFNN-AMF controller is completed.

Contents

Power Control Using PWFNN Controllers

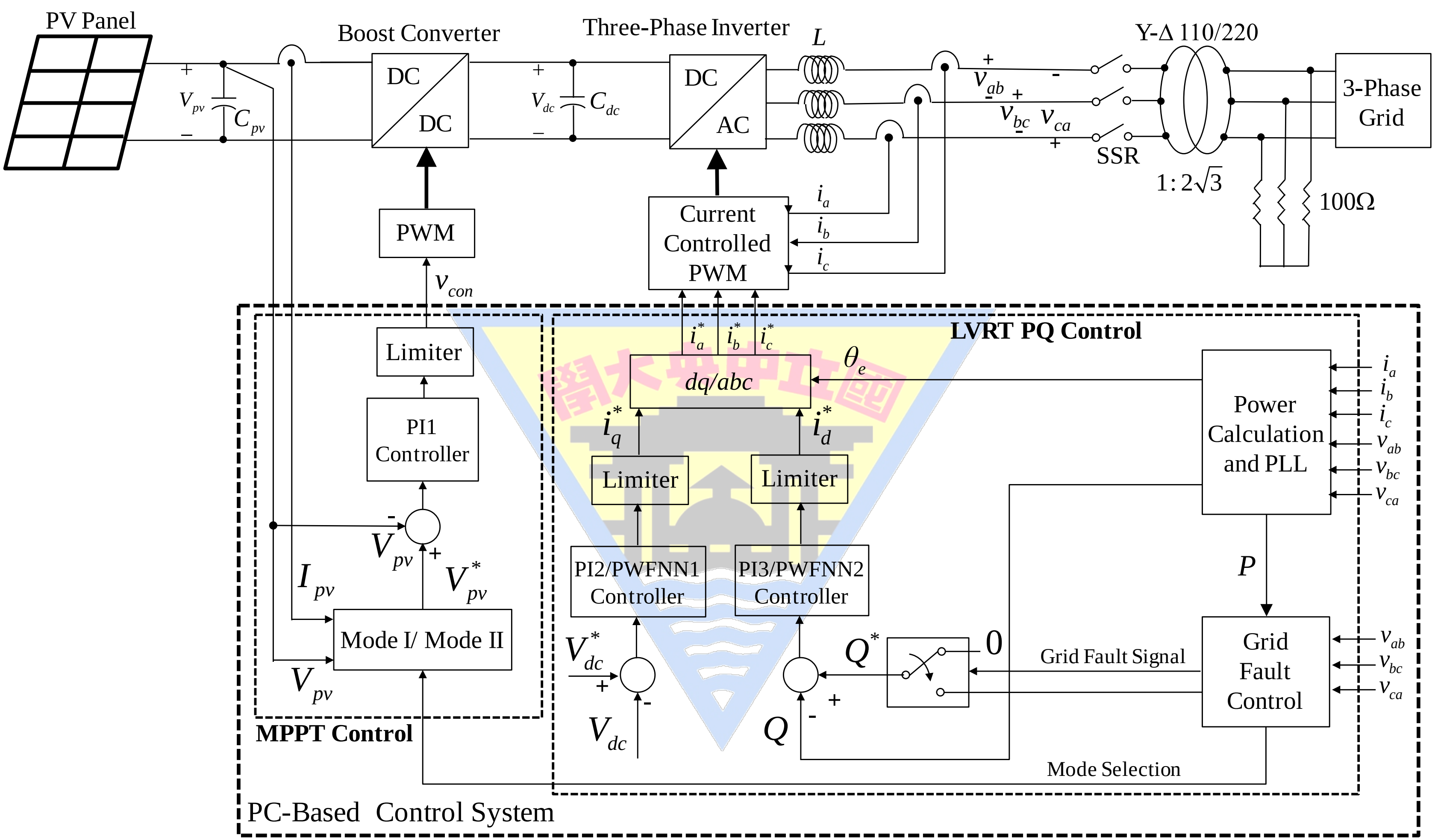

Fig. 5.1

Power Control Using PWFNN Controllers

The average tracking error T_{erravg} , the maximum tracking error T_{MAX} and the standard deviation of the tracking error T_σ for the reference tracking are defined as follows:

$$T_{err}(N) = T^*(N) - T(N) \tag{5.1}$$

$$T_{MAX} = \max_N \left(\left| T_{err}(N) \right| \right), \quad T_{erravg} = \frac{1}{m} \left(\sum_{N=1}^{m} T_{err}(N) \right) \tag{5.2}$$

$$T_\sigma = \sqrt{\frac{1}{m} \left(\sum_{N=1}^{m} \left(T_{err}(N) - T_{erravg} \right)^2 \right)} \tag{5.3}$$

Power Control Using PWFNN Controllers

Reactive Power Supporting with Boost Converter Operated at Mode I

Case 1): single phase-to-ground fault occurs with 0.5 pu voltage dip

- P_{pv}= 600 W and P = 526 W
- Q rises to 380 VAR
- voltages: 1.0 pu, 0.77 pu and 0.77 pu
- V_{pv} and I_{pv} remain unchanged due to normal operating of the MPPT control at Mode I.
- V_{mpp} = 150.7 V, irradiance = 600 W/m^2
- V_{pv} = 150.9 V, I_{pv}=4.03 A
- PI controllers:
  - ➢settling time of Q= 0.3 s, overshoot of V_{dc} = 2.6 %
- PWFNN controllers:
  - ➢settling time of Q= 0.1 s, overshoot of V_{dc} = 1.14 %

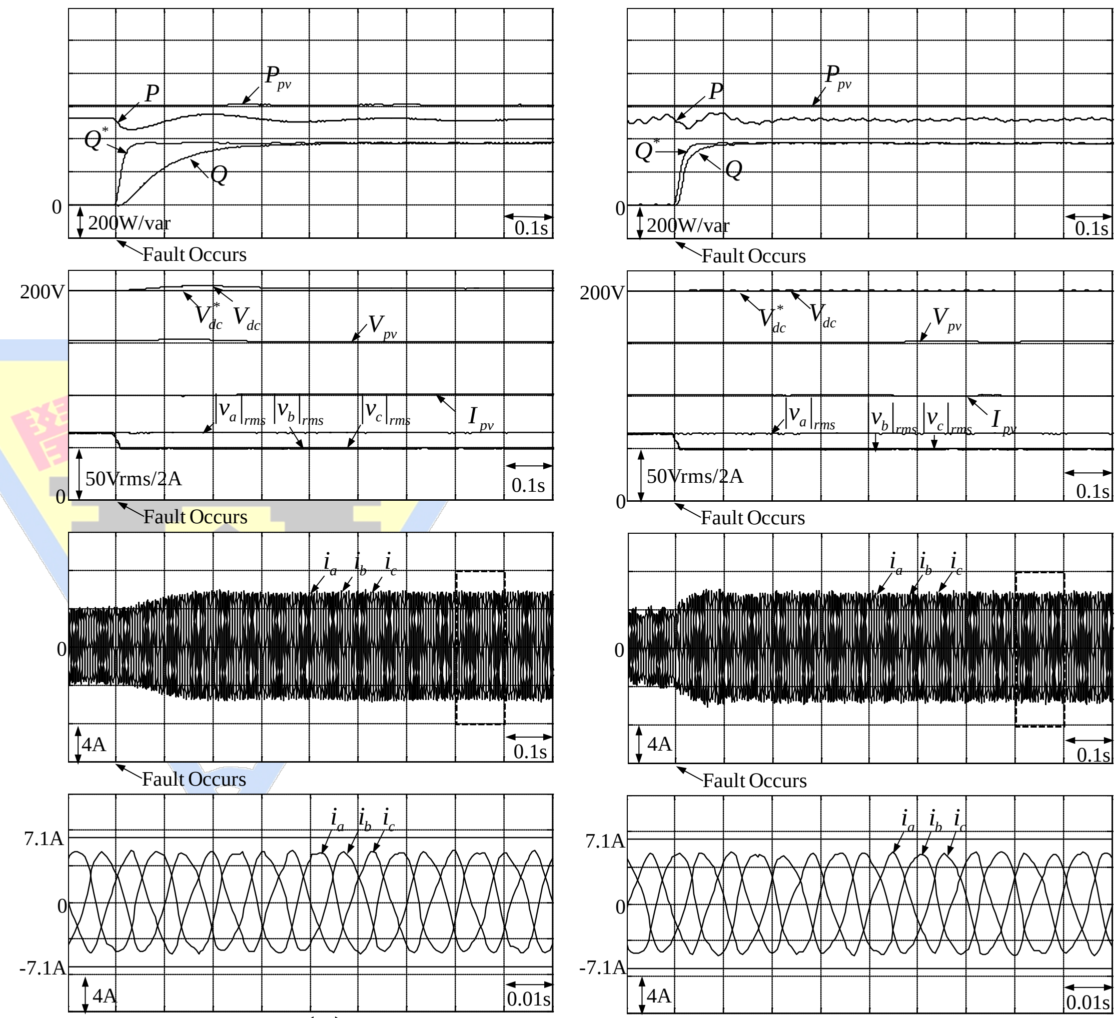

Fig. 5.2 (a) PI (b) PWFNN

Power Control Using PWFNN Controllers

Reactive Power Supporting with Boost Converter Operated at Mode II

Case 2): single phase-to-ground fault occurs with 0.5 pu voltage dip

- P_{pv}= 1000 W → 836 W
- P = 865 W → 720 W
- Q rises to 380 VAR
- voltages: 1.0 pu, 0.77 pu and 0.77 pu
- V_{pv} = 153 V → 164 V
- I_{pv} = 6.5 A → 5.1 A, at Mode II.
- PI controllers:
  - ➢settling time of Q= 0.3 s, overshoot of V_{dc} = 2.5 %
- PWFNN controllers:
  - ➢settling time of Q= 0.1 s, overshoot of V_{dc} = 1.1 %

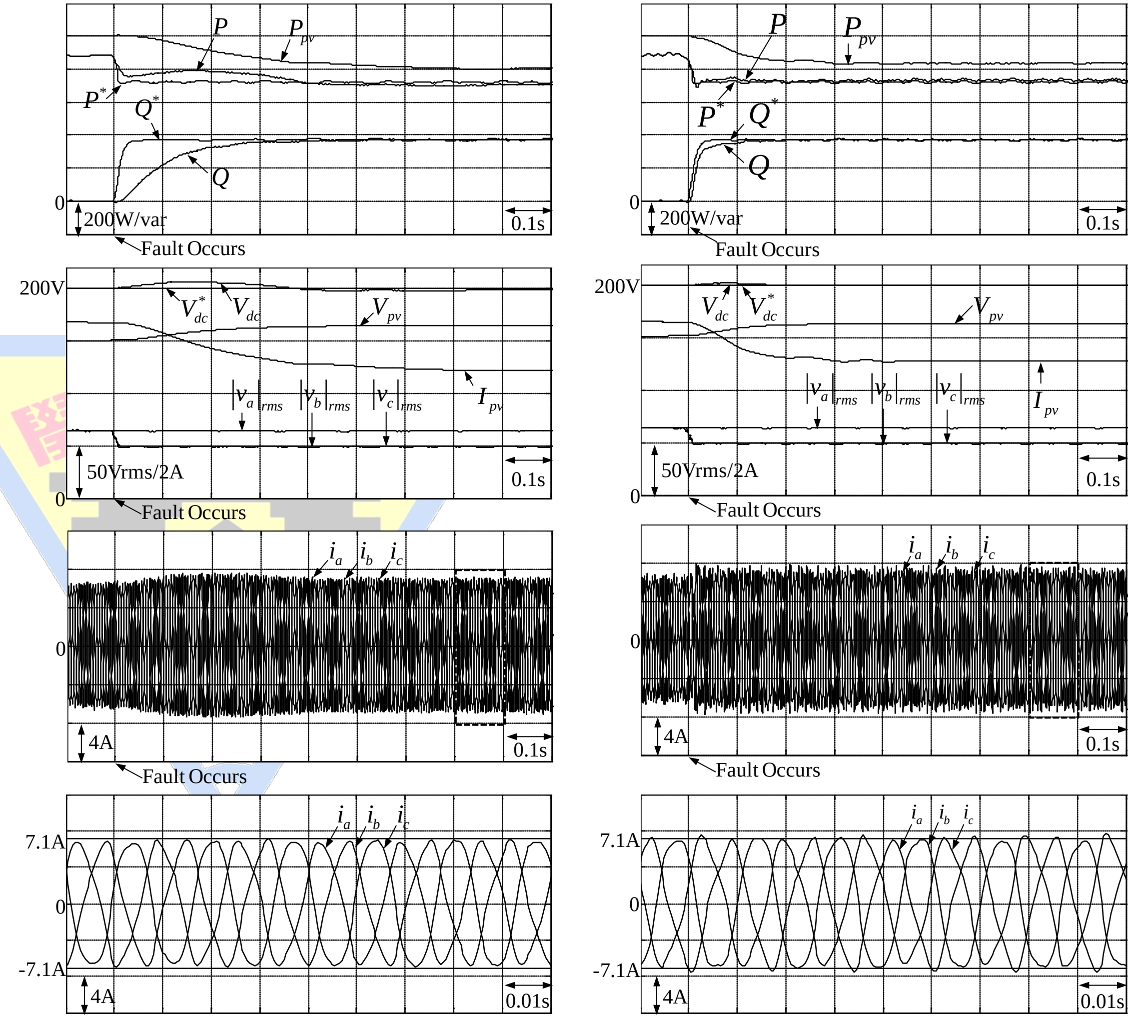

Fig. 5.3 (a) PI (b) PWFNN

Power Control Using PWFNN Controllers

Reactive Power Supporting with Boost Converter Operated at Mode II

Case 3): double phase-to-phase fault occurs with 0.5 pu voltage dip

- P_{pv}= 1000 W → 112 W
- P = 860 W → 55 W
- Q rises to 720 VAR
- voltages: 0.5 pu, 0.92 pu and 0.92 pu
- V_{pv} = 153 V → 174 V
- I_{pv} = 6.5 A → 0.62 A, at Mode II.
- PI controllers:
  - ➢settling time of Q= 0.5 s, overshoot of V_{dc} = 4.63 %
- PWFNN controllers:
  - ➢settling time of Q= 0.2 s, overshoot of V_{dc} = 6.71 %

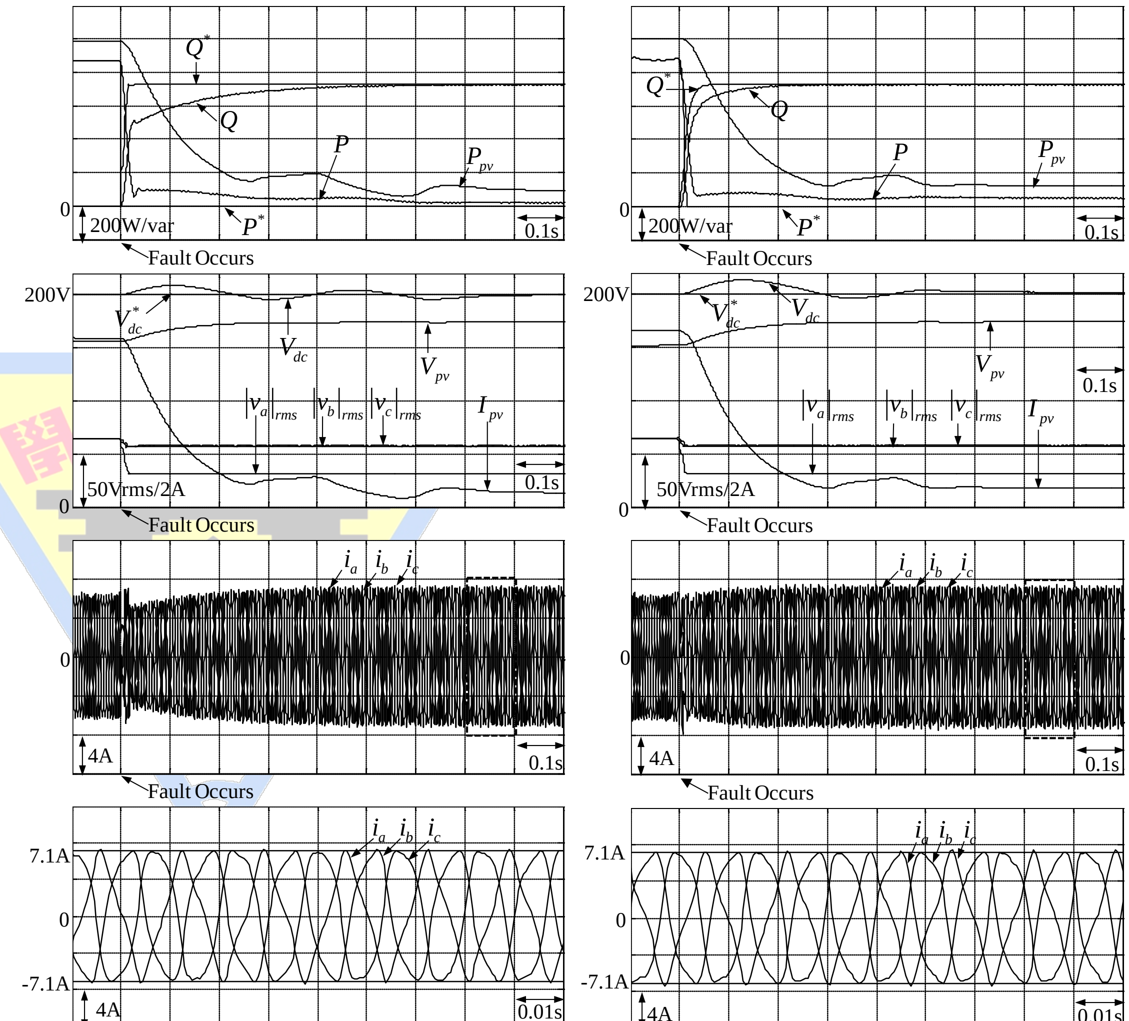

Fig. 5.4 (a) PI (b) PWFNN

Power Control Using PWFNN Controllers

Cases 1 to 3 Using FNN Controllers (1/2)

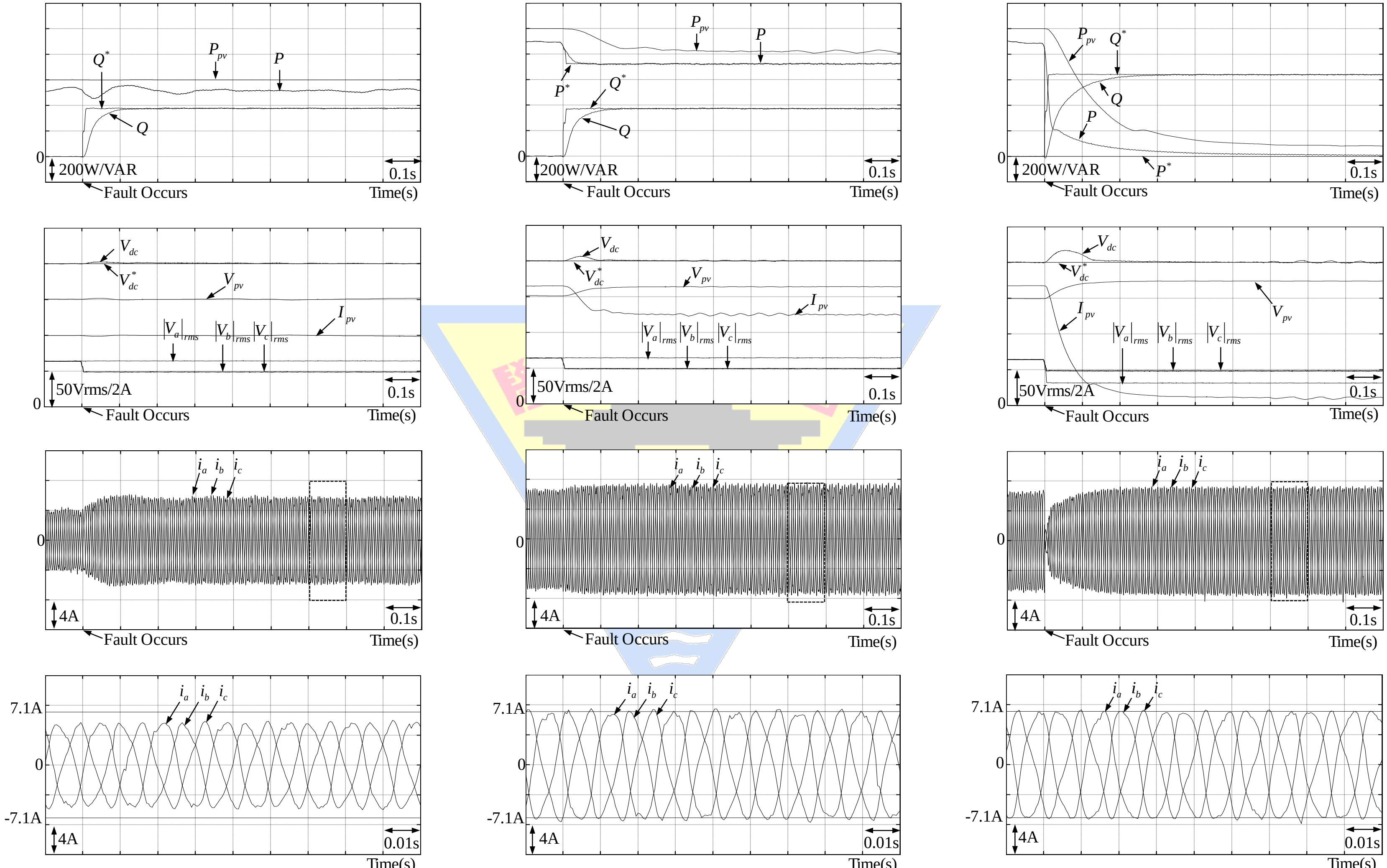

Fig. 5.5 (a) Case 1 (b) Case 2 (c) Case 3

Power Control Using PWFNN Controllers

Cases 1 to 3 Using FNN Controllers (2/2)

Case 1):

- P_{pv}= 600 W and P = 530 W
- Q rises to 378 VAR
- voltages: 1.0 pu, 0.76 pu and 0.76 pu
- V_{pv} and I_{pv} unchanged (Mode I).
- V_{mpp} = 150.5 V, irradiance = 600 W/m^2
- V_{pv} = 150.0 V, I_{pv}=3.99 A
- PI controllers:
  - settling time of Q= 0.3 s
  - overshoot of V_{dc} = 2.6 %
- FNN controllers:
  - settling time of Q= 0.12 s
  - overshoot of V_{dc} = 1.2 %
- PWFNN controllers:
  - settling time of Q= 0.1 s
  - overshoot of V_{dc} = 1.14 %

Case 2):

- P_{pv}= 1000 W → 820 W
- P = 896 W → 720 W
- Q rises to 377 VAR
- voltages: 1.0 pu, 0.76 pu and 0.76 pu
- V_{pv} = 151.2 V → 164 V
- I_{pv} = 6.6 A → 5.0 A, at Mode II.
- PI controllers:
  - settling time of Q= 0.3 s
  - overshoot of V_{dc} = 2.5 %
- FNN controllers:
  - settling time of Q= 0.15 s
  - overshoot of V_{dc} = 3.3 %
- PWFNN controllers:
  - settling time of Q= 0.1 s
  - overshoot of V_{dc} = 1.1 %

Case 3):

- P_{pv}= 1000 W → 88 W
- P = 886 W → 15 W
- Q rises to 655 VAR
- voltages: 0.5 pu, 0.91 pu and 0.9 pu
- V_{pv} = 151.4 V → 174 V
- I_{pv} = 6.6 A → 0.44 A, at Mode II.
- PI controllers:
  - settling time of Q= 0.5 s
  - overshoot of V_{dc} = 4.63 %
- FNN controllers:
  - settling time of Q= 0.25 s
  - overshoot of V_{dc} = 7.5 %
- PWFNN controllers:
  - settling time of Q= 0.2 s
  - overshoot of V_{dc} = 6.71 %

Power Control Using PWFNN Controllers

Performance Discussion

- The performance measurements of PWFNN controller are superior to the other controllers (PI, FNN).
- When the FNN and PWFNN controllers are implemented, the overshoot of V_{dc} is larger owing to more energy accumulated in C_{dc} during the transient period.
- computation complexity
  - ➢ PWFNN: 753 computation steps.
  - ➢ PI: 3 computation steps.
- implementation complexity
  - ➢ PWFNN: 427 code lines/ 14k bytes.
  - ➢ PI: only three function blocks by using Simulink.

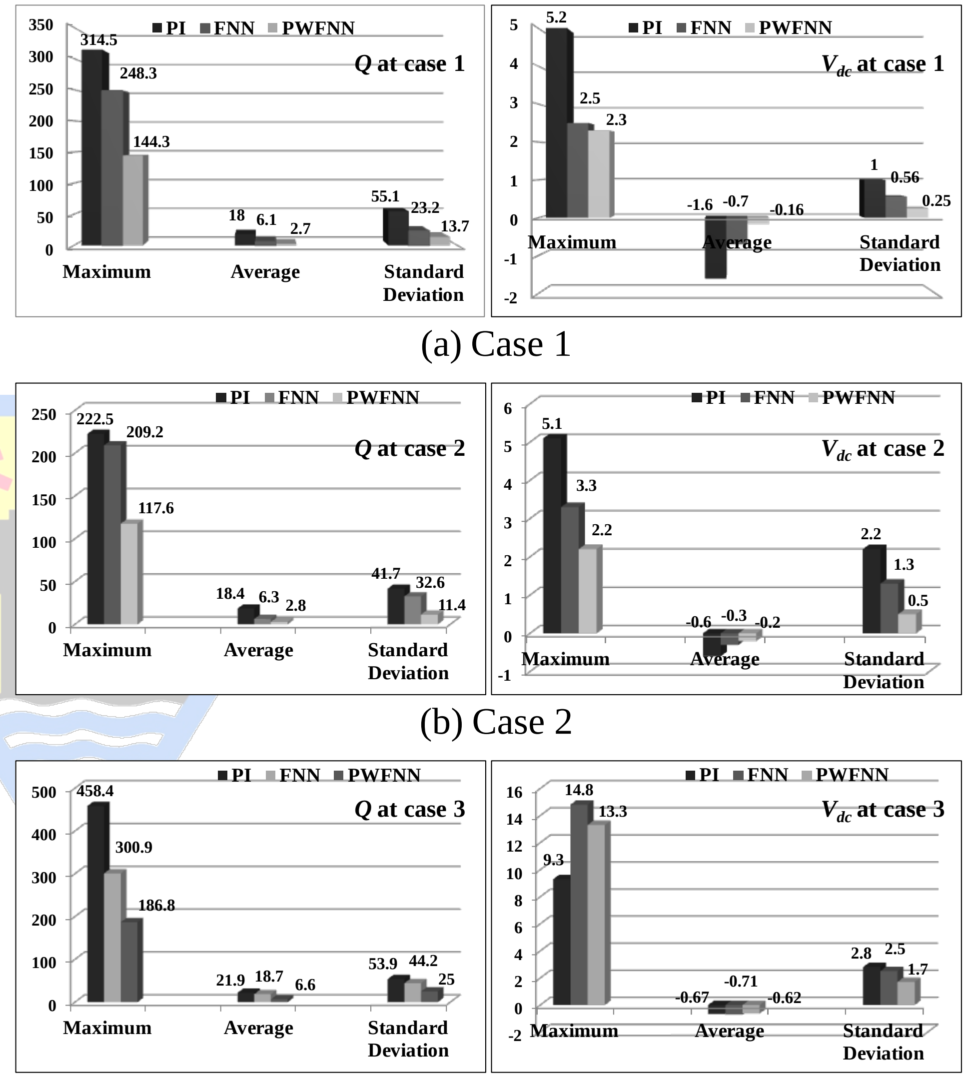

Fig. 5.6 (c) Case 3

Power Control Using PWFNN Controllers

Decreasing of Irradiance with Boost Converter Operated at Mode I

Case 4): single phase-to-ground fault occurs with 0.5 pu voltage dip

- t = 0.2 s: voltage sag occurrence
- P_{pv} = 603 W, P = 533 W (unchanged)
- Q rises to 383 VAR
- voltages: 1.0 pu, 0.77 pu and 0.77 pu
- V_{pv} = 150.3 V, I_{pv} = 4.1 A, at Mode I
- t = 1.0 s; irradiance 600 → 300 W/m^2
- P_{pv}= 603 W → 305 W
- P = 533 W → 243 W
- Q = 383 VAR (unchanged)
- V_{pv} = 151.6 V, I_{pv} = 2.1 A, at Mode I
- The irradiance change after grid fault may cause the response of P oscillating for both the PI or PWFNN controllers with stable response of Q.

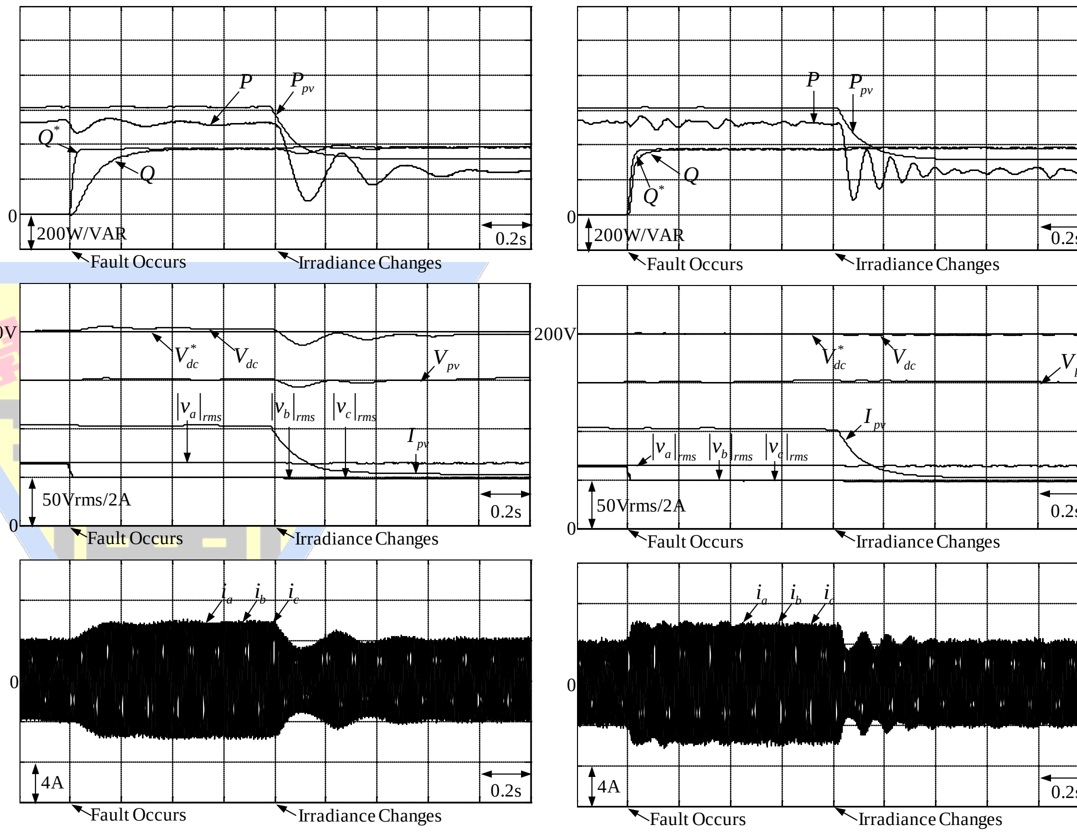

(a) PI

(b) PWFNN

Fig. 5.7

Power Control Using PWFNN Controllers

Decreasing of Irradiance with Boost Converter Operated at Mode I

<u>*Case 5)*:</u> single phase-to-ground fault occurs with 0.5 pu voltage dip

- irradiance = 30 W/m^2
- t = 0.2 s: voltage sag occurrence
- P_{pv} = 30 W, P = 0 W
- Q rises to 391 VAR
- voltages: 1.0 pu, 0.77 pu and 0.77 pu
- V_{pv} = 158.9 V, I_{pv} = 0.23 A, at Mode I
- If the output power of PV panel is less than 30 W, the generated power can't support the electronic circuits to operate and the boost converter and three-phase inverter will shut down.

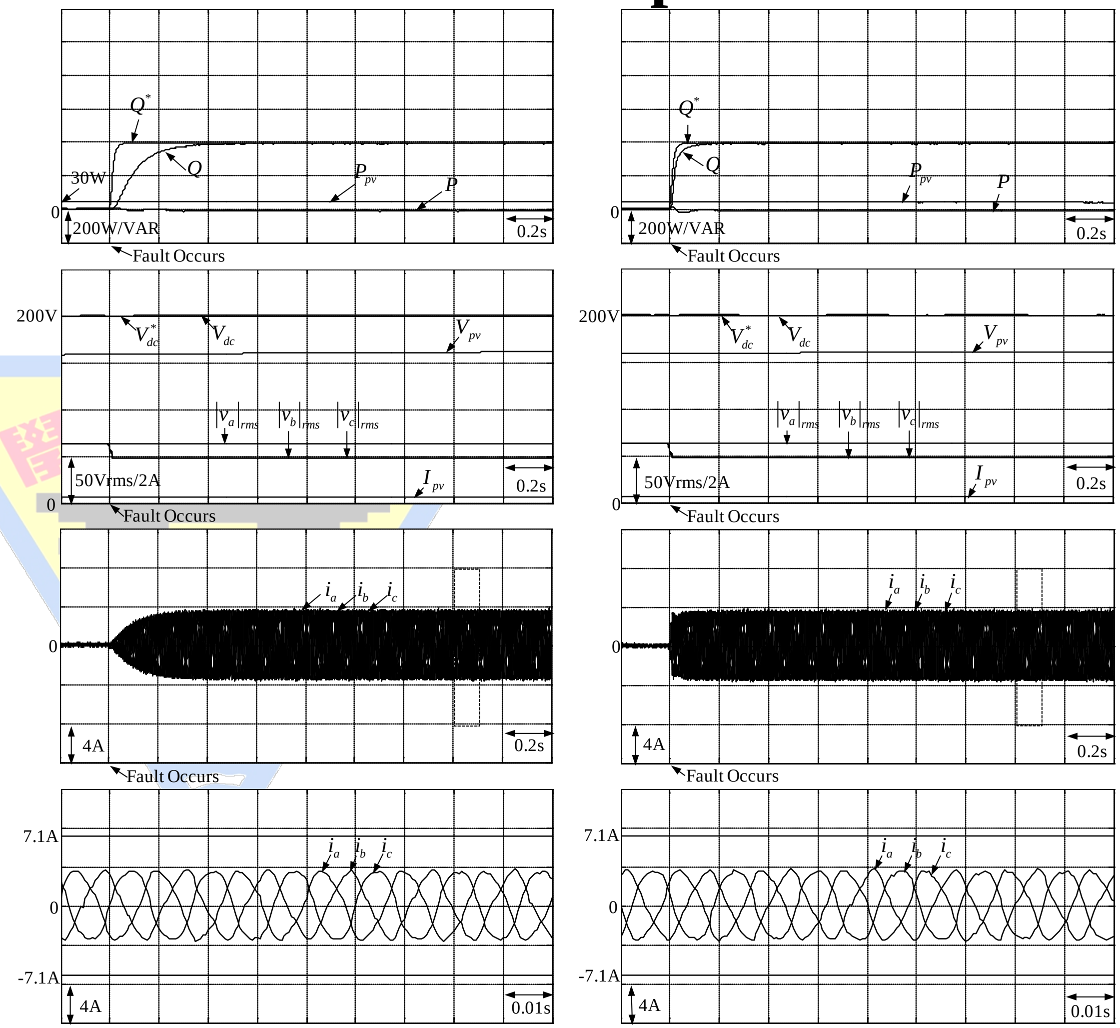

Fig. 5.8 (a) PI (b) PWFNN

Power Control Using TSKPFNN-AMF Controllers

Fig. 5.9

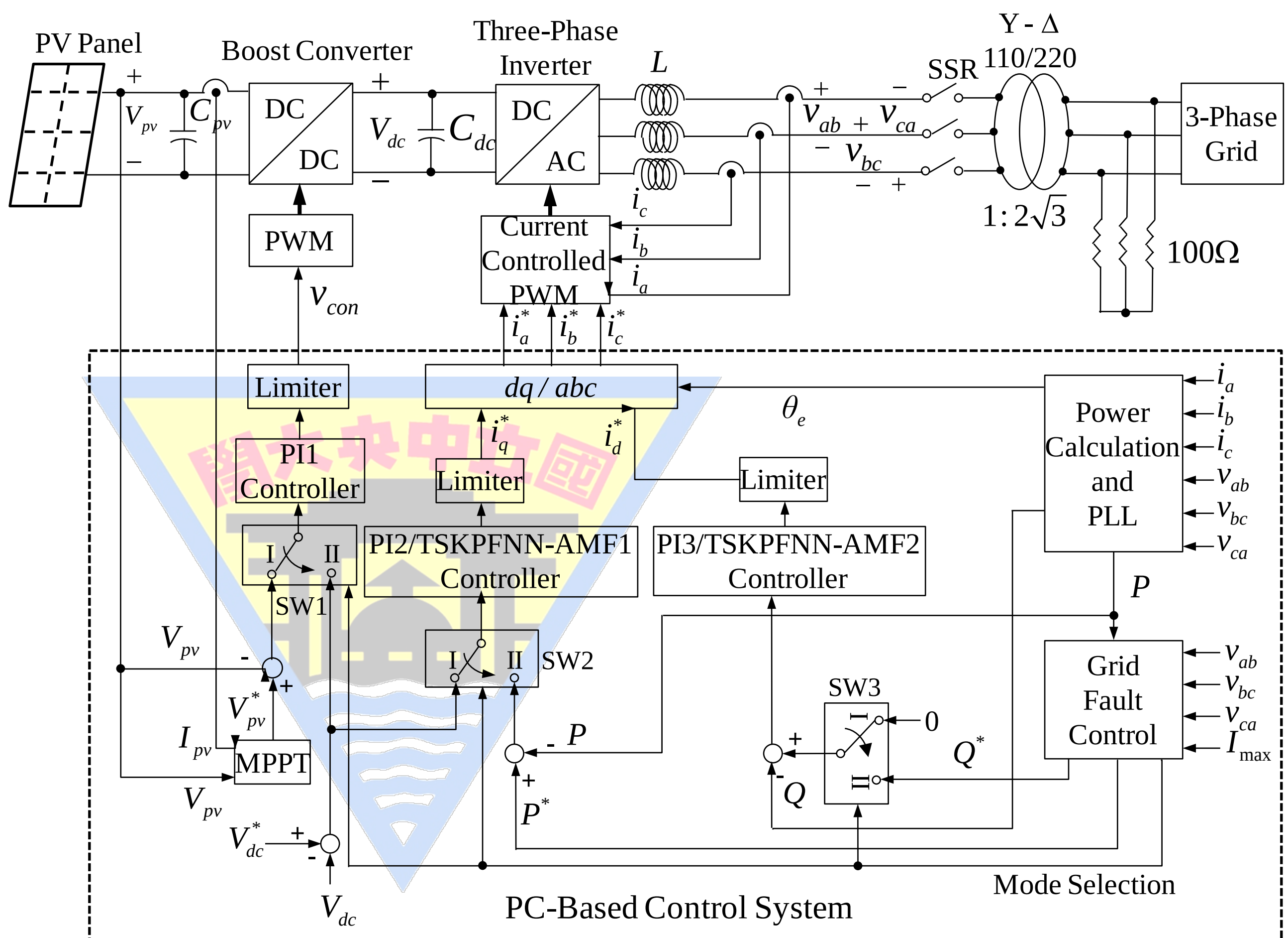

The integral of squared error (ISE) of the tracking error T_{ISE} :

$$T_{ISE} = \int_0^{\infty} \{e(t)\}^2 dt \approx \Delta T \sum_{N=1}^{m} \left(T_{err}(N)\right)^2, \quad T_{err}(N) = T^*(N) - T(N) \qquad (5.4)$$

Power Control Using TSKPFNN-AMF Controllers

Reactive Power Supporting at Mode I

<u>*Case 1):*</u> double phase-to-ground fault occurs with 0.3 pu voltage dip

- P_{pv}= 612 W and P = 524 W
- Q rises to 456 VAR
- voltages: 0.7 pu, 0.87 pu and 0.87 pu
- V_{pv} = 150.9 V, I_{pv}=4.05 A, at mode I
- i_q^* changes from 4.1 A to 4.9 A; i_d^* rises to 2.9 A
- PI controllers:
  - ➢settling time of Q= 0.45 s, overshoot of V_{dc} = 4.9 %
- TSKPFNN-AMF controllers:
  - ➢settling time of Q= 0.3 s, overshoot of V_{dc} = 1.45 %
- The settling time of Q is decreased by 33.3 % and the overshoot of V_{dc} is decreased by 70.4 % by using the TSKPFNN-AMF controllers.

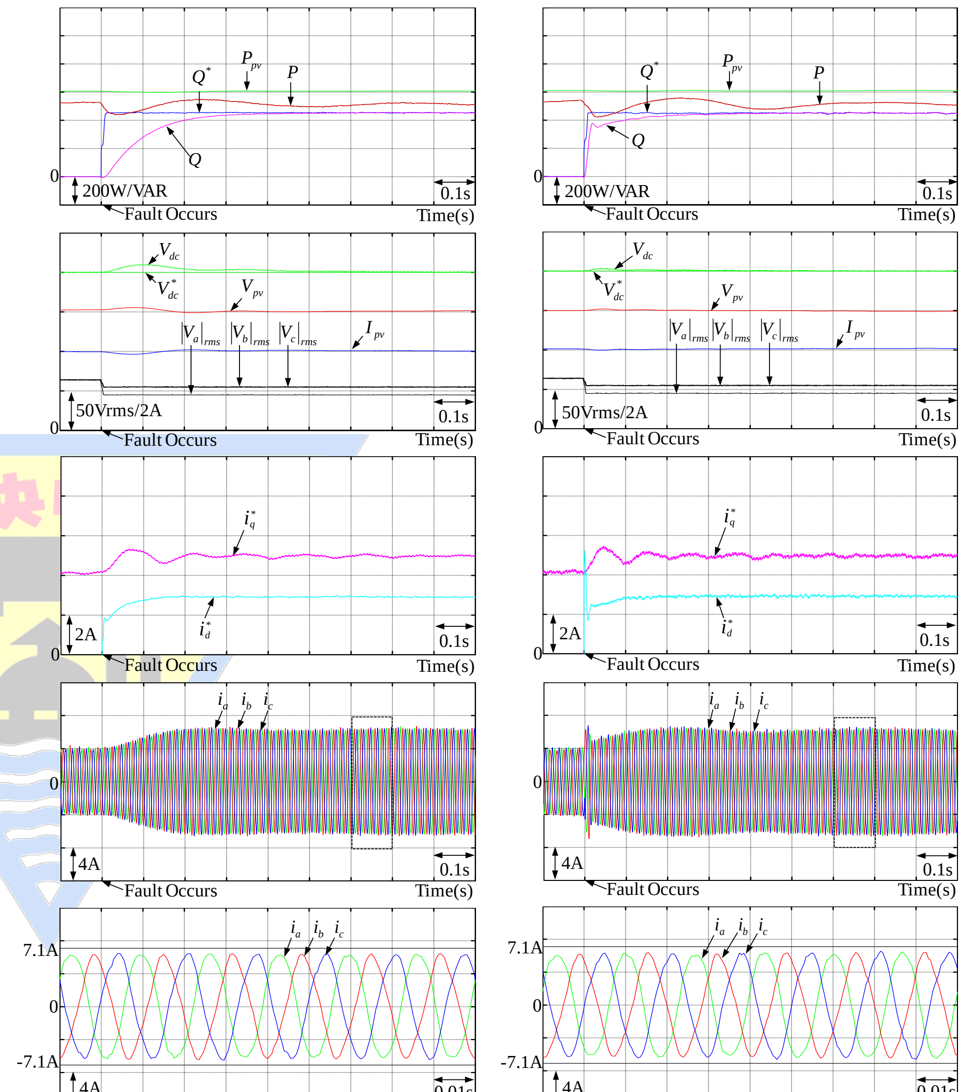

Fig. 5.10 (a) PI (b) TSKPFNN-AMF

Power Control Using TSKPFNN-AMF Controllers

Reactive Power Supporting at Mode II

Case 2): double phase-to-ground fault occurs with 0.7 pu voltage dip

- P_{pv}= 1005 W → 102 W; P = 882 W → 21 W
- Q rises to 527 VAR, , at mode II
- voltages: 0.3 pu, 0.67 pu and 0.68 pu
- V_{pv} = 150.4 → 173.9 V, I_{pv}= 6.6 → 0.52 A
- i_q^* drops from 6.2 A to 1.3 A; i_d^* rises to 5.9 A
- PI controllers:
  - ➢settling time of Q= 0.7 s, overshoot of V_{dc} = 5.4 %
- TSKPFNN-AMF controllers:
  - ➢settling time of Q= 0.16 s
  - ➢ overshoot of V_{dc} = 7 % (by PI1)
- The settling time of Q is decreased by 77.1 % by using the TSKPFNN-AMF controllers.

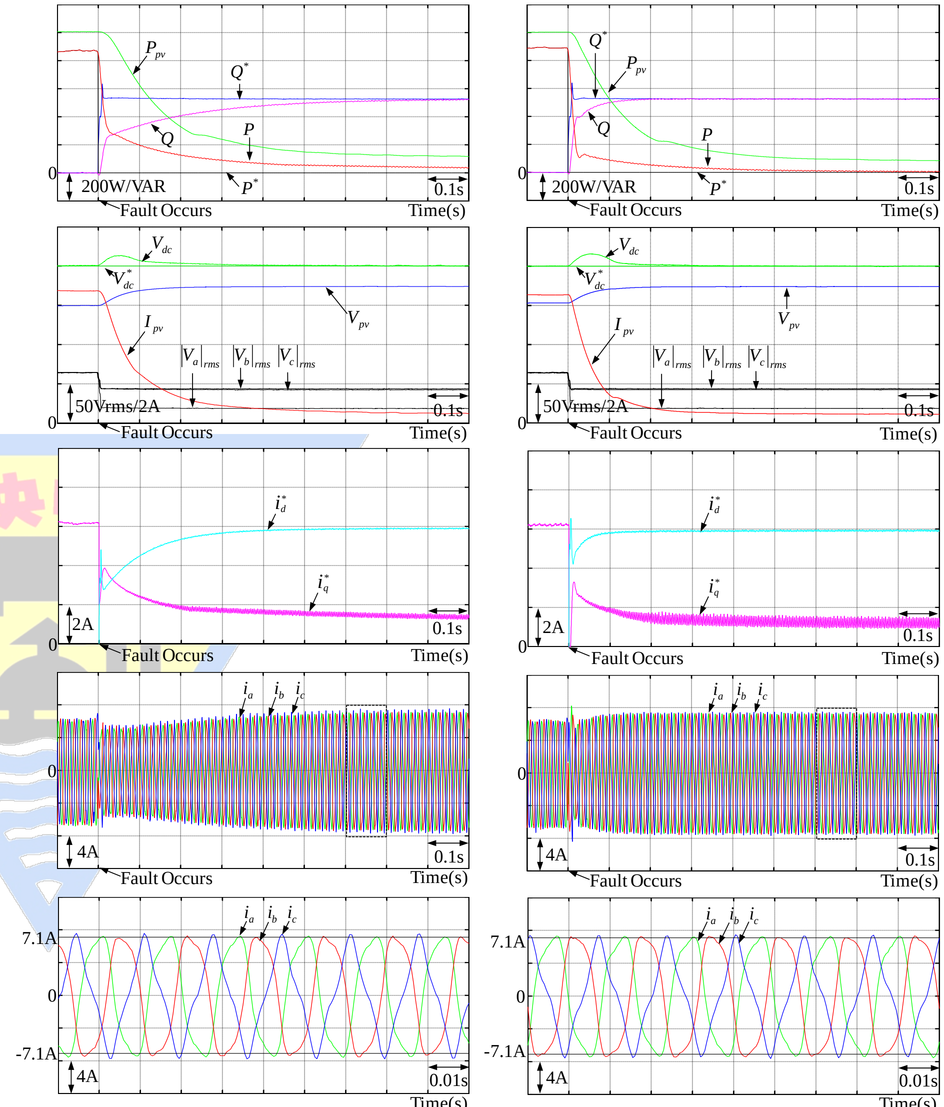

Fig. 5.11 (a) PI (b) TSKPFNN-AMF

Power Control Using TSKPFNN-AMF Controllers

Reactive Power Supporting at Low Irradiance

Case 3): double phase-to-ground fault occurs with 0.7 pu voltage dip

- Irradiance: 100 W/m^2
- P_{pv}= 106 W $\rightarrow$ 77.6 W; P = 63.8 W $\rightarrow$ 1.4 W
- Q rises to 522 VAR, , at mode II
- voltages: 0.29 pu, 0.67 pu and 0.68 pu
- V_{pv} = 158 $\rightarrow$ 168 V, I_{pv}= 0.67 $\rightarrow$ 0.46 A
- i_q^* 1.37 $\rightarrow$ 1.23 A; i_d^* rises to 5.9 A
- PI controllers:
  - ➢settling time of Q= 0.65 s, overshoot of V_{dc} = 1.9 %
- TSKPFNN-AMF controllers:
  - ➢settling time of Q= 0.2 s
  - ➢ overshoot of V_{dc} = 1.4 % (by PI1)
- The settling time of Q is decreased by 77.1 % by using the TSKPFNN-AMF controllers.

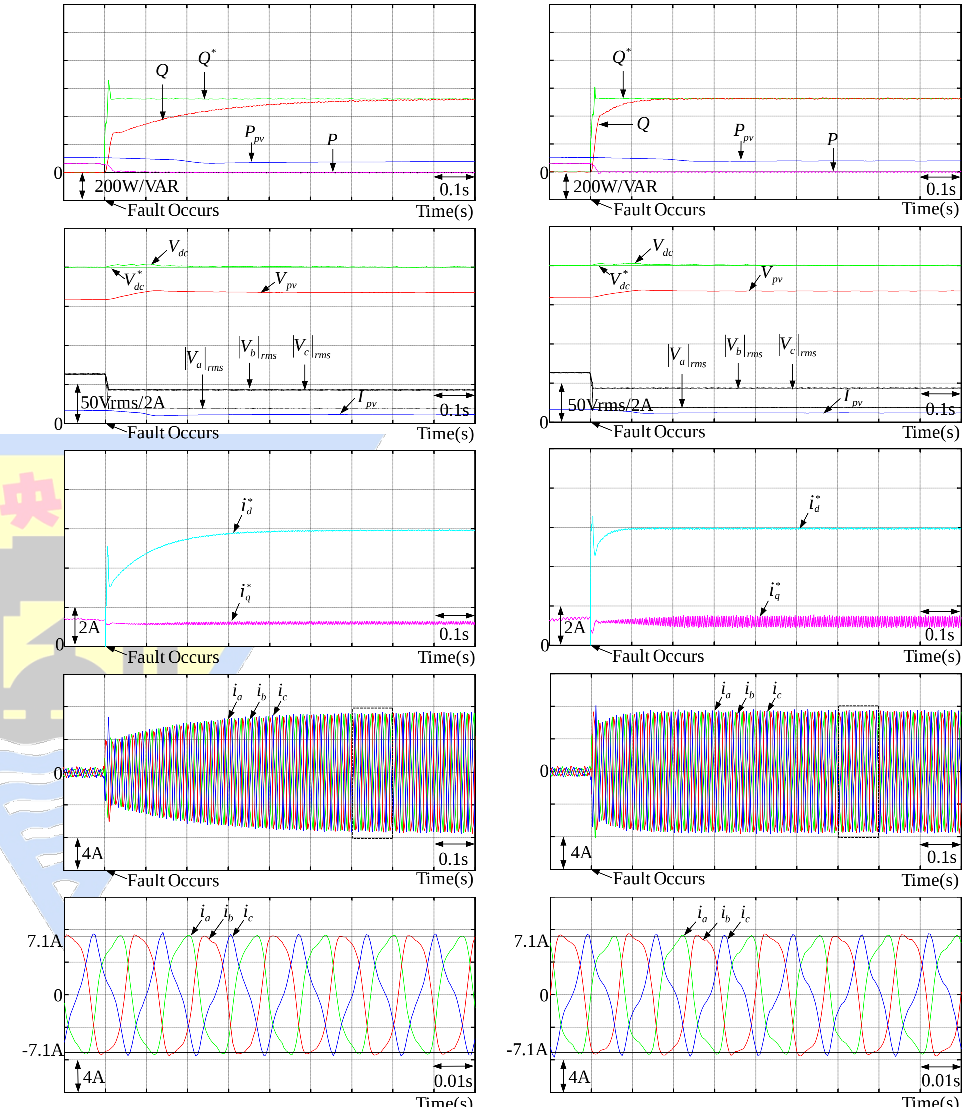

Fig. 5.12 (a) PI (b) TSKPFNN-AMF

Power Control Using TSKPFNN-AMF Controllers

Reactive Power Supporting at Unsymmetrical Unbalance Fault Condition

<u>*Case 4)*: </u>double phase-to-ground fault unsymmetrical balance fault with 0.3 pu and 0.5 pu voltage dip

- P_{pv}= 609 W → 546 W; P = 532 W → 449 W
- Q rises to 556 VAR, , at mode II
- voltages: 0.61 pu, 0.77 pu and 0.86 pu
- V_{pv} = 152 → 162 V, I_{pv}= 4.0 → 3.3 A
- i_q^* 4.1 → 4.9 A; i_d^* rises to 4.1 A
- PI controllers:
  - ➢settling time of Q= 0.45 s, overshoot of V_{dc} = 4.1 %
- TSKPFNN-AMF controllers:
  - ➢settling time of Q= 0.3 s
  - ➢ overshoot of V_{dc} = 0.6 % (by PI1)

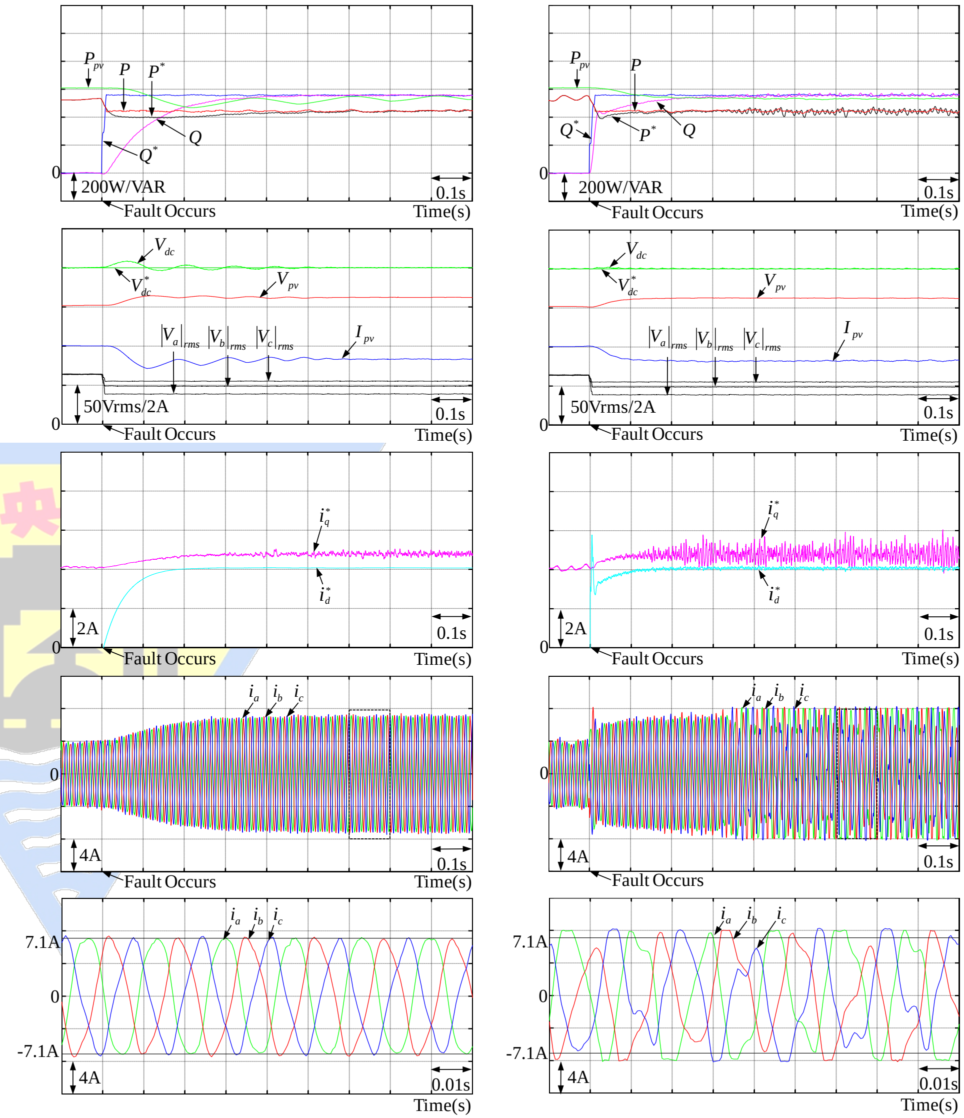

Fig. 5.13 (a) PI (b) TSKPFNN-AMF

Power Control Using PWFNN Controllers

Cases 1 and 2 Using FNN Controllers (1/2)

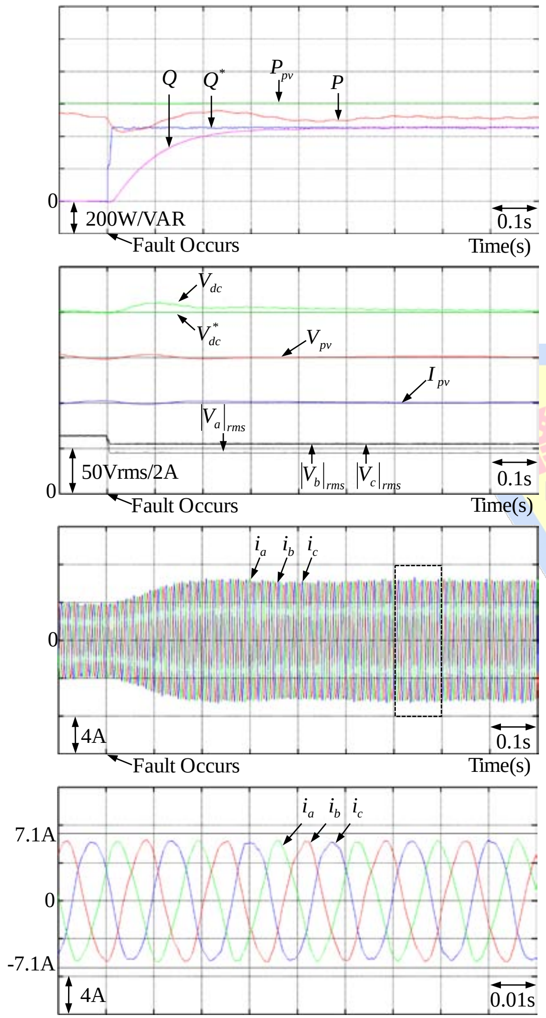

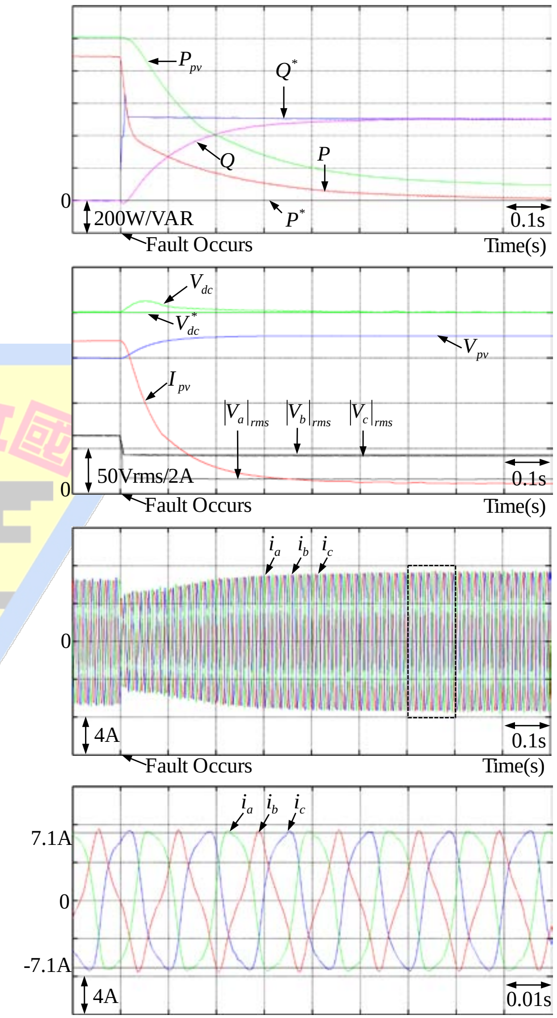

Fig. 5.14 (a) Case 1 (b) Case 2

Power Control Using PWFNN Controllers

Cases 1 and 2 Using FNN Controllers (2/2)

Case 1):

- P_{pv}= 608 W and P = 520 W
- Q rises to 457 VAR
- voltages: 0.7 pu, 0.87 pu and 0.87 pu
- V_{pv} = 150.6 V, I_{pv}=4.03 A, at mode I
- PI controllers:
  - settling time of Q= 0.45 s
  - overshoot of V_{dc} = 4.9 %
- FNN controllers:
  - settling time of Q= 0.42 s
  - overshoot of V_{dc} = 4.5 %
- TSKPFNN-AMF controllers:
  - settling time of Q= 0.3 s
  - overshoot of V_{dc} = 1.45 %.

Case 2):

- P_{pv}= 1008 W → 96 W; P = 887 W → 13 W
- Q rises to 504 VAR, , at mode II
- voltages: 0.3 pu, 0.67 pu and 0.67 pu
- V_{pv} = 151.4 → 174 V, I_{pv}= 6.6 → 0.0.46 A
- PI controllers:
  - settling time of Q= 0.7 s
  - overshoot of V_{dc} = 5.4 %
- FNN controllers:
  - settling time of Q= 0.55 s
  - overshoot of V_{dc} = 5.7 % (by PI1)
- TSKPFNN-AMF controllers:
  - settling time of Q= 0.16 s
  - overshoot of V_{dc} = 7 % (by PI1)

Power Control Using TSKPFNN-AMF Controllers

Table 5.1 THDs of Three-Phase Currents for Case 1 to Case 4

Test Case	Controller	i_a (%)	i_b (%)	i_c (%)	Average (%)
Case 1	PI	8.73	8.72	7.16	8.20
	TSKPFNN-AMF	8.23	7.23	8.82	8.09
Case 2	PI	15.98	14.24	18.26	16.16
	TSKPFNN-AMF	16.90	16.55	21.45	18.30
Case 3	PI	17.59	16.62	21.87	18.69
	TSKPFNN-AMF	20.65	18.86	26.22	21.91
Case 4	PI	9.20	10.79	11.58	10.52
	TSKPFNN-AMF	19.99	25.74	34.20	26.64

- In Case 4, the THDs of i_a, i_b, and i_c are 9.2 %, 10.79 % and 11.58 % when the PI controllers are used, and the THDs of i_a, i_b, and i_c and are 19.99 %, 25.74 %, and 34.2 % when the TSKPFNN-AMF controllers are used.

Power Control Using TSKPFNN-AMF Controllers

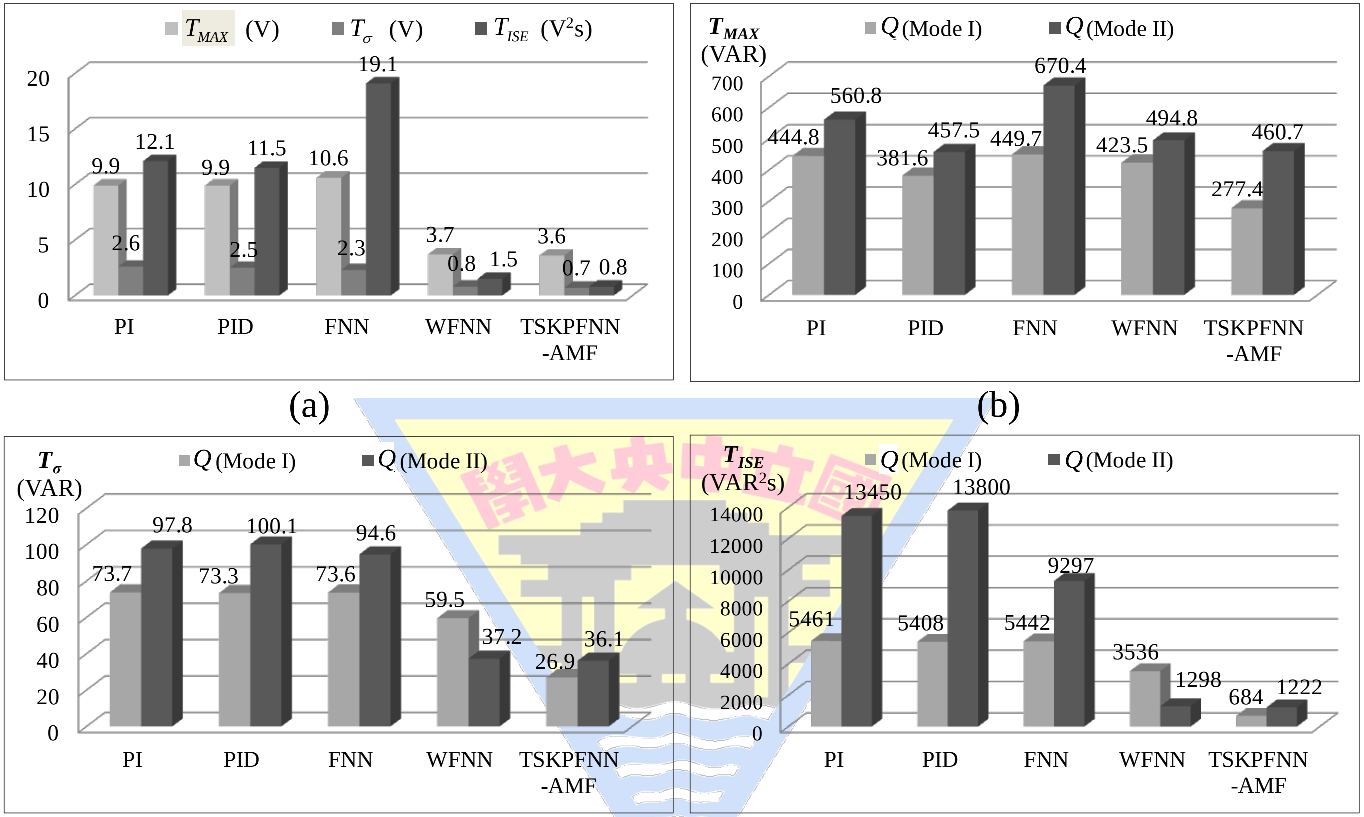

Fig. 5.15 (c) (d)

- The performances of TSKPFNN-AMF controllers are superior to the other controllers.
- Computation complexity: TSKPFNN-AMF controller: 662 steps; PI controller: 3 steps
- Implementation complexity: TSKPFNN-AMF controller: 377 code lines/ 13k bytes; PI controller: 3 blocks

Contents

Conclusions

Conclusions

- Voltages and currents analyses of PV system during the grid faults were described.
- A dual mode operation control method is developed.
- Network structure, online learning algorithms and convergence analysis.
- Performances of the proposed controllers are better than PI, PID, FNN and WFNN controllers.
- Major contributions
  - The formula for the depth of the unsymmetrical voltage sags is proposed and used to determine the injected reactive power during grid faults considering the current limit.
  - The dual mode control strategy is developed to maintain the balance of power between boost converter and three-phase inverter during grid faults
  - Two intelligent controllers are developed to control the active and reactive power of the grid-connected three-phase PV system
  - The BP-based online learning algorithm of the PWFNN and TSKPFNN-AMF controllers with self-tuning learning rates.
  - The proposed controllers are successful implemented to control the power and DC-link bus voltage of a three-phase grid-connected PV system during grid faults.

Academic Performance

Journal Papers

[1] F. J. Lin, K. C. Lu, and B. H. Yang, “Recurrent Fuzzy Cerebellar Model Articulation Neural Network Based Power Control of Single-Stage Three-Phase Grid-Connected Photovoltaic System during Grid Faults,” *IEEE Trans. Industrial Electronics*, revised, 2016. (SCI)

[2] F. J. Lin, K. C. Lu, T. H. Ke, and Y. R. Chang, “Probabilistic Wavelet Fuzzy Neural Network Based Reactive Power Control for Grid-Connected Three-Phase PV System during Grid Faults Renewable Energy,” *Renewable Energy*, vol. 92, pp. 437-449, 2016. (SCI)

[3] F. J. Lin, K. C. Lu, T. H. Ke, and H. Y. Li, “Reactive Power Control of Three-Phase PV System during Grids Faults Using Takagi-Sugeno-Kang Probabilistic Fuzzy Neural Network Control,” *IEEE Trans. Industrial Electronics*, vol. 62, no. 9, pp. 5516-5528, 2015. (SCI)

[4] F. J. Lin, K. C. Lu, T. H. Ke, and Y. R. Chang, “Reactive Power Control of Single-Stage Three-phase Photovoltaic System during Grid Faults Using Recurrent Fuzzy Cerebellar Model Articulation Neural Network,” *International Journal of Photoenergy*, vol. 2014, Article ID 760743, 13 pages, 2014. (SCI)

Patents

[1] F. J. Lin, K. C. Lu, and H. Y. Lee, *Photovoltaic Power Generation System*, USA Patent, US 9,276,498 B2, March 2016

[2] F. J. Lin, K. C. Lu, and H. Y. Lee, *Photovoltaic Energy Power Generation System*, Patent No. I522767, R. O. C., Feb. 2016